

~~CONFIDENTIAL~~

NACA RM A50F06

A 50 F 06

6317

TECH LIBRARY KAFB, NM

0142936



~~CONFIDENTIAL~~  
NACA

# RESEARCH MEMORANDUM

LIFT AND PITCHING-MOMENT INTERFERENCE BETWEEN A POINTED  
CYLINDRICAL BODY AND TRIANGULAR WINGS OF VARIOUS

ASPECT RATIOS AT MACH NUMBERS OF 1.50 AND 2.02

By Jack N. Nielsen, Elliott D. Katzen, and Kenneth K. Tang

Ames Aeronautical Laboratory  
Moffett Field, Calif.



CLASSIFIED DOCUMENT

~~Information affecting the National Defense of the United States within the meaning of the Espionage Laws, the transmission or the revelation of its contents in any manner to an unauthorized person is prohibited by law.~~  
Information so classified may be imparted to personnel performing essential services of the United States, appropriate civilian officers and employees of the Federal Government, and to United States citizens of known loyalty and discretion who are authorized to receive such information.

## NATIONAL ADVISORY COMMITTEE FOR AERONAUTICS

WASHINGTON

September 12, 1950

319.98/13

~~CONFIDENTIAL~~



## NATIONAL ADVISORY COMMITTEE FOR AERONAUTICS

RESEARCH MEMORANDUM

LIFT AND PITCHING-MOMENT INTERFERENCE BETWEEN A POINTED  
CYLINDRICAL BODY AND TRIANGULAR WINGS OF VARIOUS  
ASPECT RATIOS AT MACH NUMBERS OF 1.50 AND 2.02

By Jack N. Nielsen, Elliott D. Katzen, and Kenneth K. Tang

## SUMMARY

In order to investigate the effects of interference on wing-body combinations, tests were conducted at Mach numbers of 1.50 and 2.02 of a pointed, cylindrical body, of six triangular wings having aspect ratios from 0.67 to 4.00, and of the wings and the body in combination. The body had a fineness ratio of 7.33, a conical nose with a semiapex angle of  $15^\circ$ , and an ogival transition section to a cylindrical afterbody. The wings had 8-percent-thick double-wedge sections with the maximum thickness at the midchord, and the wing-body combinations were made by inserting the wings at zero incidence into the cylindrical part of the body. Experimental lift and pitching-moment results were obtained for a nominal angle-of-attack range of  $\pm 5.5^\circ$  and a constant Reynolds number, based on the body length, of 5.5 million. Theoretical characteristics of the body and wings alone and in combination, as well as the interference, were calculated from the available theories and compared with the experimental results.

The experimental results presented have been corrected for the non-uniform flow conditions that existed in the wind tunnel and the theoretical method by which the corrections were made is given.

The theory described by Allen in NACA RM A9I26, 1949, produced results in good agreement with the measured values of lift and pitching moment for the body. The agreement was better at a Mach number of 1.50 than at 2.02. Comparison of the wing-alone data with the results of Love in NACA RM L9D07, 1949, indicated a marked effect of the position of maximum thickness on the lift-curve slope. The lift-curve slopes for the wings tested were considerably greater than for wings with the maximum thickness at 18-percent chord in the upper range of wing aspect ratios. For the wing-body combinations having low-aspect-ratio wings, the theoretical predictions of Spreiter in NACA TN 1662, 1948, were in good agreement with the experimental values of lift and moment. For the wing-body combinations having higher-aspect-ratio wings, a modification of the theory of NACA TN 1662 produced predictions in good agreement with experiment.

The results for the components alone and in combination were used to determine the total interference, which is defined as the sum of the interference effects of the body on the wing forces and of the wings on the body forces. The interference effects were important for the wing-body combinations having small wings relative to the body. Both the results of the theory of NACA TN 1662 and of the modified theory were in good agreement with the experimentally measured interference results.

## INTRODUCTION

The forces on a combination of a wing and a body can be considered to consist of the sum of the forces on the wing alone, the body alone, and the interference forces of the wing on the body and of the body on the wing. The wing alone and the body alone have received intensive study, but at the present time no correlation exists between theory and experiment for the interference forces, even though these forces may be large.

Several investigators have presented theoretical methods of predicting interference forces. Spreiter, in reference 1, has investigated the effect of interference on the lift-curve slope and center-of-pressure position of slender wing-body combinations. This theory assumes that the body is slender and the leading edges of the wings are swept well behind the Mach cone. Ferrari, in reference 2, has investigated the problem of interference between a rectangular wing and a body. In this paper the effect of the wing on the body forces, assuming that the flow field due to the wing is unchanged by the presence of the body, and the effect of the body on the wing forces, assuming that the body flow field is unchanged by the presence of the wing, were determined. Brown, Friedman, and Hodes, in reference 3, have investigated the conical-flow problem of interference between a triangular wing and a conical body, the apex of which coincides with the wing apex.

The present experiments were designed to measure the total lift and pitching-moment interference of triangular wing-body combinations at supersonic speeds and to compare the data with the theory and a modification of the theory of reference 1. The experiments also afforded an opportunity for comparison of the lift force and pitching moment of the body and wings alone with values predicted by the available theories. The total interference, which is defined as the sum of the interference effects of the body on the wing forces and of the wing on the body forces, was determined by subtracting the sum of the lift, or pitching moment, of the wings and body alone from the lift, or pitching moment, of the corresponding combinations. In order to isolate the interference effect of the body on the wings from the effect of the wings on the body, the forces on the wings must be measured in the presence of the body; the experimental program includes the measurement of these forces and will be reported in a subsequent paper.

## NOTATION

A	wing aspect ratio
$A_p$	plan-form area of body ( $2 \int_0^l adx$ ), square inches
a	local body radius, inches
$\bar{c}$	mean aerodynamic chord $\left(\frac{2}{3} c_r\right)$ , inches
$cd_c$	cross-flow section drag coefficient of a circular cylinder
$C_L$	lift coefficient based on total wing plan-form area for wings and combinations and on base area for body
$\Delta C_{L_s}$	increment in lift coefficient due to stream angle
$C_m$	pitching-moment coefficient about wing centroid for wings and combinations and about body nose for body, based on total wing plan-form area and mean aerodynamic chord for wings and combinations, and on base area and body length for body
$\Delta C_{m_s}$	increment in moment coefficient due to stream angle
$c_r$	wing apex chord, inches
E	complete elliptic integral of second kind
L	lift force, pounds
l	body length, inches
$\frac{L_{WB}+L_{BW}}{L_B+L_W}$	total lift-interference ratio $\left(\frac{L_{WB}+L_{BW}}{L_B+L_W} = \frac{L_C}{L_B+L_W} - 1\right)$
M	pitching moment, inch-pounds
$M_0$	free-stream Mach number
$\frac{M_{WB}+M_{BW}}{M_B+M_W}$	total moment-interference ratio, moments about body nose $\left(\frac{M_{WB}+M_{BW}}{M_B+M_W} = \frac{M_C}{M_B+M_W} - 1\right)$

$\frac{\Delta p}{q}$	loading coefficient, ratio of difference between lower- and upper-surface static pressures and free-stream dynamic pressure
s	local wing semispan, inches
S	total wing plan-form area as extended in figure 1 ( $S = c_r s_m$ ), square inches
V	volume of body, cubic inches
$V_0$	free-stream velocity, inches per second
x	longitudinal coordinate, measured along body axis from body nose for body alone and combination, or measured along wing apex chord from wing apex for wings, positive downstream, inches
y	lateral coordinate, normal to vertical plane of symmetry, inches
$\alpha$	angle of attack in radians unless otherwise specified
$\alpha_s$	stream angle, radians
$\beta$	$\sqrt{M_0^2 - 1}$
$\epsilon$	wing semiapex angle, degrees
$\lambda$	modification factor to account for finite wing aspect ratios
$\eta$	correction for three-dimensional effects on body
$\Lambda_0$	sweep angle of wing leading edge, degrees
$\Lambda_{1/2}$	sweep angle of wing midchord line, degrees
$\phi$	velocity potential

## Subscripts

B	body alone
W	wing alone
C	wing-body combination
WB	effect of wing on body

BW	effect of body on wing
$L \rightarrow 0$	limiting value of quantity as lift approaches zero
b	value at body base
l	value at intersection of wing leading edge and body
m	maximum value
s	value due to stream angle
t	value at the wing trailing edge
$\infty$	theoretical value for infinite aspect ratio
bc	centroid of body plan-form area
cp	center of pressure of wing-body combination

#### EXPERIMENTAL CONSIDERATIONS

##### Apparatus and Procedure

The tests were performed in the Ames 1- by 3-foot supersonic wind tunnel No. 1. This closed-circuit continuous-operation wind tunnel is equipped with a flexible-plate nozzle that can be adjusted to give test-section Mach numbers from 1.2 to 2.4. Reynolds number variation is accomplished by changing the absolute pressure in the tunnel from one-fifth of an atmosphere to approximately three atmospheres depending on the Mach number and ambient temperature. The tunnel is equipped with a strain-gage balance for measuring the aerodynamic forces on sting-supported models (reference 4). In the arrangement described in reference 4, the pitching moment was obtained from the reactions on the main balance springs and was not sufficiently accurate. Therefore, the pitching moment in the present investigation was more accurately determined from strain-gage measurements of the bending moment in the sting support (reference 5).

The models were tested through a nominal angle-of-attack range of  $\pm 5.5^\circ$  at Mach numbers of 1.50 and 2.02. A constant Reynolds number of 0.5 million per inch was maintained and, in order to make the effects of condensation negligible, the humidity was held to less than 0.0003 pound of water vapor per pound of dry air.

## Models and Supports

The body (fig. 1) had a fineness ratio of 7.33, a conical nose with a semiapex angle of  $15^{\circ}$ , and an ogival transition section fairing into a cylindrical afterbody. The length of the body was limited by the condition that the nose wave reflected from the tunnel side walls should fall behind the body base.

The geometrical properties and designations of the six wing models used in the investigation are summarized in table I. A photograph of the wing family is presented in figure 2. The wings had symmetrical double-wedge airfoil sections in the streamwise direction with a maximum thickness of 8 percent at the midchord. All the wings were made of hardened tool steel and were finished by grinding. They were all equipped with small supports which were designed to reduce the effect of the supports on the aerodynamic forces of the wing alone to a negligible quantity.

For all the wing-body combinations the wings were located along the cylindrical part of the body. The method of assembling the combinations is shown in figure 3.

All the models were mounted on the same sting. However, as shown in figure 4, different shrouds were used for the wing tests than for the body and combination tests.

## ANALYSIS OF DATA

### Corrections to Experimental Results

The experimental lift and moment data have been corrected for the nonuniform flow conditions in the tunnel test section. The measured values of the stream angle and pressure coefficient in the vertical plane of symmetry of the empty tunnel were used, together with the theoretical results of the appendix, in estimating the corrections. It was found, in general, that the corrections to lift and moment were small but not negligible. The maximum correction to lift-curve slope for all configurations at both Mach numbers was 10 percent of the measured lift-curve slope. The corrections to the moment data, at both Mach numbers, shifted the center of pressure of the body 4 percent of the body length; the center of pressure of the wings, a maximum of 3 percent of the wing mean aerodynamic chord; and the center of pressure of the wing-body combinations, a maximum of 3 percent of the body length.

[REDACTED]

### Precision

The precision of the experimental data has been evaluated by the method outlined in Appendix A of reference 5. This includes an estimate of the precision of each measurement and the resulting uncertainty in the measurement. There is a further uncertainty involved in the accuracy of the corrections applied to the experimental data of the present tests. The latter inaccuracy is estimated to cause an uncertainty of  $\pm 0.007$  in the lift coefficients for body, wings, and wing-body combinations; an uncertainty of  $\pm 0.006$  in the moment coefficients for the body and an uncertainty of  $\pm 0.004$  in the moment coefficients for the wings and the wing-body combinations. The total uncertainty in the results is taken as the square root of the sum of the squares of the individual uncertainties.

The following table lists the total uncertainty for all configurations at both Mach numbers:

Quantity	Uncertainty for body	Uncertainty for wings and wing-body combinations
$M_0$	$\pm 0.02$	$\pm 0.02$
$C_L$	$\pm .009$	$\pm .009$
$C_m$	$\pm .007$	$\pm .005$
$\alpha(\text{deg})$	$\pm .10$	$\pm .10$

### THEORETICAL CONSIDERATIONS

#### Body

Tsien (reference 6) showed that the lift force and pitching moment on slender bodies of revolution at low angles of attack are the same at supersonic speeds as at subsonic speeds, and that the results are the same as those predicted by Munk's airship theory (reference 7). Thus, the lift-curve slope of a body with a finite base is 2 for all Mach numbers if the base is used as the reference area. Experiments have shown that, while this is a good approximation at low angles of attack, at higher angles of attack the lift-curve slope increases and the slender-body theory is no longer adequate. Slender-body theory neglects the effects of viscosity and considers only the potential flow about the body. A large

[REDACTED]

effect of viscosity can be included by considering the flow of a real fluid about an infinite cylinder inclined to the stream. In reference 8, Jones has shown that the forces on an inclined infinite cylinder are determined by the cross flow, that is, the component of the flow perpendicular to the cylinder. Since the flow of a real fluid normal to a cylinder usually separates, a drag of cross flow occurs and appears as a normal force on the inclined cylinder. Allen (reference 9) has estimated the effects of cross-flow separation on the aerodynamic coefficients of slender bodies of revolution. The lift coefficient, by the method of reference 9, is

$$C_L = 2\alpha + \frac{A_p}{\pi a_b^2} c_{d_c} \eta \alpha^2 \quad (1)$$

The first term represents the contribution of slender-body theory. The second term accounts for the added lift due to the cross-flow separation. In the second term  $c_{d_c}$  is the drag coefficient experienced by an infinitely long circular cylinder at the Reynolds number and Mach number based upon the diameter of the body and the cross component of the velocity. The factor  $\eta$  allows for the effect of the finite length of the circular cylinder with the assumption that the reduction in drag coefficient for fineness ratio is the same for each element of the cylinder. It is also assumed that the reduction in drag is the same for a body (of varying cross section) and a cylinder of equal fineness ratios. For a cylinder with the same fineness ratio as the present body, reference 9 gives  $\eta=0.65$ . This value, together with  $c_{d_c}=1.2$ , has been used with equation (1) in determining the theoretical lift curve for the body.

If the moments are taken about the nose and the body length is used as the reference length, the pitching-moment coefficient is given by

$$C_m = 2\alpha \left( \frac{V}{\pi a_b^2 l} - 1 \right) - \eta c_{d_c} \frac{A_p}{\pi a_b^2} \alpha^2 \frac{x_{bc}}{l} \quad (2)$$

### Wings

The lift-curve slopes for the wings were determined from the results of the linearized supersonic wing theory (references 10 or 11). When the parameter  $\beta \tan \epsilon$  is less than unity (subsonic leading edge), the lift-curve slope is given by

$$\frac{dC_L}{d\alpha} = \frac{2\pi \tan \epsilon}{E(\sqrt{1-\beta^2} \tan^2 \epsilon)} \quad (3)$$

For the triangular wings for which  $\beta \tan \epsilon$  is greater than unity (supersonic leading edge), the lift-curve slope is given by (reference 12)

$$\frac{dC_L}{d\alpha} = \frac{4}{\beta} \quad (4)$$

Linear theory gives the result that the pitching-moment coefficient with the moment taken about the centroid of the wing plan-form area is zero for all triangular wings having symmetrical sections.

#### Wing-Body Combinations

The lift-curve slope for a slender wing-body combination consisting of a low-aspect-ratio triangular wing mounted on the cylindrical part of a pointed body is by the method of Spreiter (reference 1)

$$\frac{dC_L}{d\alpha} = \frac{2\pi a_b^2}{s_m^2} \tan \epsilon + 2\pi \left( 1 - \frac{a_b^2}{s_m^2} \right)^2 \tan \epsilon \quad (5)$$

where the total wing plan-form area (including the part within the body) has been used as the reference area. The first term in equation (5) represents the contribution of the body nose to the lift, and the second term represents the contribution of the winged part of the configuration. The lift force on the cylindrical afterbody is considered to be zero. This would be correct for combinations having low-aspect-ratio wings, provided the trailing vortex sheet remained flat. When the effects of higher-aspect-ratio wings and the rolling up of the trailing vortex sheet are considered in the analysis, the force on the afterbody is no longer zero, but estimates show that the force is negligible for the angles of attack of the present tests.

In order to extend the method of reference 1 for application to combinations consisting of triangular wings of higher aspect ratio, the second term in equation (5) must be modified. When the method of Spreiter is applied to wings alone, the results become identical to the low-aspect-ratio triangular-wing results of Jones (reference 13). It is known that the lift-curve slopes estimated by this theory are too large when the parameter  $\beta \tan \epsilon$  is not small compared to unity and must be multiplied by a factor  $\lambda$  to bring them into agreement with the linearized theories applicable to triangular wings of higher aspect ratio. The factor  $\lambda$  is obtained by dividing equations (3) and (4) by the low-aspect-ratio results ( $dC_L/d\alpha = 2\pi \tan \epsilon$ ):

$$\left. \begin{aligned} \lambda &= \frac{1}{E(\sqrt{1-\beta^2 \tan^2 \epsilon})}; & \beta \tan \epsilon &\leq 1 \\ \lambda &= \frac{2}{\pi\beta \tan \epsilon}; & \beta \tan \epsilon &\geq 1 \end{aligned} \right\} \quad (6)$$

The assumption is now made that the wing factor  $\lambda$  can be applied to the lift on the winged part of the combinations. Theoretically, this assumption has been shown to be valid for the conical flow case of a triangular wing mounted on a conical body, the apex of which coincides with the wing apex (reference 1). By physical reasoning, this assumption is a good approximation for small values of  $\beta \tan \epsilon$  (the range where the theory of reference 1 should be applicable) since  $\lambda$  is then nearly unity. It is also good when the lift on the winged part of the combination is carried mostly by the wing, which is the case if  $\beta \tan \epsilon$  is large when the wing is large relative to the body. By the application of the factor  $\lambda$  to equation (5), there is obtained

$$\frac{dC_L}{d\alpha} = \frac{2\pi a_b^2}{s_m^2} \tan \epsilon + 2\pi\lambda \left(1 - \frac{a_b^2}{s_m^2}\right)^2 \tan \epsilon \quad (7)$$

This equation has been used to determine the modified theory values of lift-curve slope for the wing-body combinations.

By the use of the foregoing method, the value of  $dC_m/dC_L$  for moments taken about the wing centroid with the mean aerodynamic chord as reference length is given as follows:

$$\frac{dC_m}{dC_L} = \frac{\left(\frac{3}{2}\right) \frac{a_b^2}{s_m^2} \left[ \frac{(x_t-l)}{c_r} + \frac{V}{\pi a_b^2 c_r} - \frac{1}{3} \right] + \frac{\lambda}{2} \left(1 - \frac{a_b^2}{s_m^2}\right)^2 \left[ \left(1 - \frac{a_b^2}{s_m^2}\right) \left(1 + \frac{3a_b^2}{s_m^2}\right) - \left(1 + \frac{a_b^2}{s_m^2}\right)^2 \right]}{\frac{a_b^2}{s_m^2} + \lambda \left(1 - \frac{a_b^2}{s_m^2}\right)^2} \quad (8)$$

The position of the center of pressure with respect to the nose of the body is given by

$$\frac{x_{cp}}{l} = \frac{\frac{a_b^2}{s_m^2} \left(1 - \frac{v}{\pi a_b^2 l}\right) + \lambda \left(1 - \frac{a_b}{s_m}\right)^2 \left[ \frac{x_t}{l} \left(1 + \frac{a_b}{s_m}\right)^2 - \frac{c_r}{3l} \left(1 - \frac{a_b}{s_m}\right) \left(1 + 3 \frac{a_b}{s_m}\right) \right]}{\frac{a_b^2}{s_m^2} + \lambda \left(1 - \frac{a_b^2}{s_m^2}\right)^2} \quad (9)$$

## RESULTS AND DISCUSSION

In order to isolate the total interference ratio  $\frac{L_{WB}+L_{BW}}{L_B+L_W}$ , the characteristics of the body alone, the wings alone, and the combinations must be measured. The results of the tests to determine these characteristics are discussed individually and are presented in the form of lift and pitching-moment coefficients in figures 5 to 7 for the body, wings, and combinations, respectively. The results are summarized in table II. From these data, the total interference was determined and the results are presented in figure 8 in terms of the total lift-interference ratio and in figure 9 in terms of the total moment-interference ratio.

### Body

Lift.— At  $M_0=1.50$ , the experimental curve (fig. 5) was in good agreement with the curve predicted by the theory of reference 9. At  $M_0=2.02$ , the experimental lift coefficients were greater in magnitude than the theoretical values at any angle of attack, consequently the experimental value of the lift-curve slope at zero angle of attack was greater than the theoretical. Since cross-flow separation does not affect  $(dC_L/d\alpha)_{L \rightarrow 0}$ , the difference between the theoretical and experimental values of this quantity must be attributed to other effects of viscosity or to the fact that the body was not sufficiently slender to warrant the use of slender-body theory. With regard to other effects of viscosity, it is known that Reynolds number can have a large effect on the value of  $(dC_L/d\alpha)_{L \rightarrow 0}$  of a body of revolution (reference 4), but it was found that for the present body  $(dC_L/d\alpha)_{L \rightarrow 0}$  was independent of scale above a Reynolds number of  $3 \times 10^6$  (based on the body length) for  $M_0=1.50$ . Since the Reynolds number was  $5.5 \times 10^6$  for the data presented at both  $M_0=1.50$  and  $M_0=2.02$ , it is believed that the scale effect was insignificant.

Pitching moment.— On the basis of slender-body theory, the center of pressure of the present body is approximately 19 percent of the body length behind the nose. According to the theory of reference 9, a force due to cross-flow separation, proportional to the square of the angle of attack, has been assumed to act at the centroid of the body plan-form area.

As the angle of attack increases, the cross force due to separation causes the center of pressure to move rearward, producing a stabilizing influence, as the theoretical curve of figure 5 shows. A comparison at the two Mach numbers of the experimental moment curve with the viscous theoretical curve shows that the agreement was good and there was little change with Mach number.

### Wings

Lift.— The lift results for the wings alone are summarized in figure 10. The wing lift-curve slopes are divided by the two-dimensional lift-curve slopes and are shown as a function of  $\beta \tan \epsilon$ . The experimental results obtained by Love (reference 14) for triangular wings with the same thickness ratio as the present wings (8 percent), but with the maximum thickness at 18 percent of the chord instead of 50 percent of the chord, are also shown in figure 10. The Reynolds numbers in the tests of reference 14 were not greatly different from those of the present tests. Comparison of the present results with those of reference 15 shows that the lift-curve slope was much less in the upper range of  $\beta \tan \epsilon$  for the wings which had steeper leading-edge wedge angles than those of the present wings. Thus, airfoil-section shape has a decided effect on the lift of triangular wings. When the flow perpendicular to the leading edge is considered, the bow wave should become attached to the wing leading edge at lower values of  $\beta \tan \epsilon$  for the present wings than for wings with maximum thickness at 18 percent of the chord. Better agreement with the linear theory is thus to be expected in this range of  $\beta \tan \epsilon$  for the present wings. According to the linear theory, the wing lift-curve slope should fall on one line when plotted as shown in figure 10. The present experimental results at Mach numbers of 1.50 and 2.02 did not fall on one line, thus additional effects of Mach number beyond those predicted by the linear theory were indicated. Why these effects of Mach number should be important for the present wings and not for the wings with maximum thickness at 18 percent of the chord is not clear.

Center of pressure.— The experimental variation of center-of-pressure position with  $\beta \tan \epsilon$  is presented in figure 11. The data show that the center-of-pressure positions were 3 to 8 percent of the mean aerodynamic chord forward of the wing centroid of area for all the wings of the present investigation except  $W_1$  at  $M_0=1.50$  and 2.02 and  $W_2$  at  $M_0=1.50$ . The results were not greatly different for the two Mach numbers. In general, the center-of-pressure positions for the wings of the present tests were slightly forward of those for the wings of reference 14. The deviation of the center of pressure from the theoretical position at the wing centroid and the deviation between wings of different section must be due to higher-order compressibility and viscous effects. A complete explanation of the deviation must await a careful study of the boundary-layer behavior on the wings, together with experimental determinations of the wing-pressure distributions.

### Wing-Body Combinations

Lift.— The lift-curve slopes of the wing-body combinations are shown in figure 12 as a function of the wing parameter  $\beta \tan \epsilon$ . The figure shows that the experimental results were in good agreement with the theoretical results of reference 1 in the low range of values of  $\beta \tan \epsilon$  for which the theory was intended. The agreement between the experimental results and the modified theoretical results was good throughout the test range. It thus appears that the modified theory should be applicable to wing-body combinations similar to those of the present tests — that is, to those configurations for which the lift of the wings is large compared to that of the body in the upper range of  $\beta \tan \epsilon$ . The method would thus be applicable to a triangular-wing airplane. However, for the case of a small surface of large  $\beta \tan \epsilon$  such that the lift of the surface is small compared to that on the body, it cannot be assumed that the present method would give valid results.

Center of pressure.— The center-of-pressure positions at zero lift, as fractions of the body length behind the nose, have been plotted against  $\beta \tan \epsilon$  for both Mach numbers in figure 13. The figure includes the theoretical center-of-pressure positions calculated by the method of reference 1 for the combinations with the low-aspect-ratio wings, and by the method of the modified theory for all the combinations. The figure shows a rapid rearward movement of the center of pressure as  $\beta \tan \epsilon$  increased, and at high values of  $\beta \tan \epsilon$  the center of pressure approached a constant position at  $x/l = 0.60$ . Since the moment was due primarily to the wings as  $\beta \tan \epsilon$  became large, the center of pressure for the combinations should approach asymptotically the limiting rearward position of the centroid for the wing family. This corresponds to  $0.636 l$  behind the nose. The agreement between theory and experiment was good. The experimental values for  $M_0=2.02$  and large values of  $\beta \tan \epsilon$  were slightly greater than the theoretical values, but never by more than 2 percent of the body length.

### Interference Effects

The lift of a wing-body combination may be defined by

$$L_C = L_W + L_B + L_{WB} + L_{BW} \quad (10)$$

where the wing alone is defined as the total wing, including the part blanketed by the body. The term  $L_{BW}$  is defined as the difference between the lift force on the wing in the presence of the body and the lift force on the wing alone. Thus  $L_{BW}$  is the effect of the body on the wing lift force. Similarly,  $L_{WB}$  is the effect of the wing on the body lift force. The total lift-interference ratio is

$$\frac{L_{WB}+L_{BW}}{L_B+L_W} = \frac{L_C}{L_B+L_W} - 1 \quad (11)$$

and, correspondingly, the total pitching-moment interference ratio is

$$\frac{M_{WB}+M_{BW}}{M_B+M_W} = \frac{M_C}{M_B+M_W} - 1 \quad (12)$$

with all moments taken about the body nose. Thus the total interference ratios may be obtained from the characteristics of wings alone, body alone, and combinations.

Lift.— Figure 8 reveals that the total lift-interference ratio was negative (i.e., unfavorable) throughout the test range. It must be remembered, however, that the sign of this ratio depends to a large extent on the wing definition. In the present paper, the wing alone included the part inside the body. If the wing had been defined as the exposed half-wings joined together, the total lift interference would have been favorable, but of the same order of magnitude. The figure also shows that the interference ratio was largest in magnitude for the combinations having the lowest ratio of the wing semispan to body radius. The interference ratio decreased rapidly as the wing semispan was increased relative to the body radius. For large values of  $s_m/a_b$ , the interference ratio approached zero.

Even though the results of reference 1 were not derived for wing-body combinations having wings of high aspect ratio, there is little difference between the results calculated by this method and those calculated by the modified theory when they are plotted in the form shown. The experimental values of the interference ratio were smaller in magnitude than the theoretical values, but the agreement between theory and experiment is considered good. Better agreement is to be expected for a body of higher fineness ratio and thinner wings than those used in the present investigation.

Pitching moment.— Figure 9 shows that, in general, the total moment-interference ratio was negative (i.e.,  $M_C < M_B+M_W$ ) and decreased in magnitude rapidly as  $s_m/a_b$  was increased. For values of  $s_m/a_b$  greater than about 3.0 the interference ratio was negligible. The experimental values of the interference ratio were less in magnitude than the theoretical values, but the agreement between experiment and theory was considered good. Figure 9 also shows that there was little difference in the moment-interference results for the two Mach numbers.

## CONCLUSIONS

In order to evaluate interference, the lift and pitching moment of a pointed cylindrical body, of six triangular wings having aspect ratios of 0.67 to 4.00 and of the wings and body in combination were investigated experimentally at Mach numbers of 1.50 and 2.02. The experimental results for the body, wings, and combinations, as well as the interference results, were compared with values predicted by available theories. The results support the following conclusions:

1. The lift and pitching-moment curves of the body as predicted by the method of NACA RM A9126, 1949, were in good agreement with the experimental curves.
2. Comparison of the results of the present investigation with those in NACA RM L9D07, 1949, indicated that the position of the maximum thickness had a marked effect on the lift of triangular wings having double-wedge sections with a maximum thickness ratio of 8 percent. For the present wings of high aspect ratio and maximum thickness at 50-percent chord, the lift-curve slopes were considerably greater than those for wings with maximum thickness at 18-percent chord.
3. For the wing-body combinations having low-aspect-ratio wings, the theoretical predictions of NACA TN 1662, 1948, were in good agreement with the experimental lift and pitching-moment results.
4. For the wing-body combinations having higher-aspect-ratio wings, the theoretical results of NACA TN 1662 were modified and found to be in good agreement with the experimental results. This modified theory should be applicable to wing-body combinations similar to those of the present tests - that is, to those configurations for which the lift of the wings is large compared to that of the body.
5. The interference effects were important for the wing-body combinations having small wings relative to the body. Both the theoretical results of NACA TN 1662 and the modified theoretical results were in good agreement with the measured values.

Ames Aeronautical Laboratory,  
National Advisory Committee for Aeronautics  
Moffett Field, Calif.

## APPENDIX

## DERIVATION OF CORRECTIONS FOR STREAM NONUNIFORMITIES

The aerodynamic coefficients of the present investigation have been corrected for nonuniform flow conditions at the tunnel position where the models were tested. Corrections were applied to account for vertical and horizontal pressure gradients and for stream angle. Although the corrections were not negligible, they were not sufficiently large to warrant more refined methods in their calculation.

In reference 1, the velocity potential  $\phi$  for the steady-state flow around an infinite cylinder having flat-plate wings was derived and used to determine the lift and pitching moment of slender wing-body combinations. It was shown that the theory is applicable to triangular wing-body combinations at supersonic speeds, provided the body is slender and has a pointed nose and the wing is swept well behind the Mach cone. The loading coefficient for a wing-body combination in a uniform stream was given in reference 1 as

$$\frac{\Delta p}{q} = \frac{4}{V_0} \frac{\partial \phi}{\partial x} = \frac{4}{V_0} \left( \frac{\partial \phi}{\partial s} \frac{ds}{dx} + \frac{\partial \phi}{\partial a} \frac{da}{dx} \right) \quad (A1)$$

The lift on a spanwise strip of width  $dx$  was given as

$$\frac{d}{dx} \left( \frac{L}{q} \right) = 2 \left[ \int_0^a \left( \frac{\Delta p}{q} \right)_B dy + \int_a^s \left( \frac{\Delta p}{q} \right)_W dy \right] \quad (A2)$$

In a nonuniform stream, the loading on models is affected by both the stream-angle magnitude and the stream-angle gradient. The magnitude of the stream angle can be accounted for by substituting equation (A1) in equation (A2) and integrating. This substitution was made in reference 1 for various configurations and the results are directly applicable to the present corrections if  $\alpha_s$  is substituted for  $\alpha$  in finding the lift on a spanwise strip of width  $dx$  due to the stream-angle magnitude at the strip. An additional loading term to account for a stream-angle gradient in the  $x$  direction is

$$\frac{\Delta p}{q} = \frac{4}{V_0} \frac{\partial \phi}{\partial \alpha_s} \frac{d\alpha_s}{dx} \quad (A3)$$

The lift on a spanwise element of the configuration due to the gradient of stream angle in the  $x$  direction can be found by substituting equation (A3) in equation (A2) and integrating. The total increment in lift

due to stream angle can then be found by adding the spanwise incremental lift due to stream-angle gradient and stream-angle magnitude and integrating the result in the  $x$  direction.

### Body Corrections

The lift and pitching-moment coefficients of the body have been corrected for stream angle, vertical pressure gradients, and for cross-flow separation due to stream angle in planes perpendicular to the body axis. For purposes of making these corrections, the flow about the body has been viewed in planes perpendicular to the body axis as shown in figure 14. Consider point  $P$  in such a plane with the tunnel empty. There will be a certain pressure coefficient at point  $P$  due to conditions in its fore-cone. With the body in place, the pressure coefficient at point  $P$  is the sum of the pressure coefficient in the empty tunnel modified by the shielding effect of the body plus the pressure disturbance due to flow around the body. The shielding effect will be a complicated function of how pressure disturbances arising in the shadow of the body from  $P$  pass around the body to  $P$ . It is believed that the shielding effect is small if  $P$  is some distance from the body. Therefore, superimposed on the pressure coefficient at  $P$  in the empty tunnel is the increment due to the flow around the body. In slender-body theory, the flow in a plane perpendicular to the body depends only on the component of the free-stream velocity in this plane together with the streamwise gradient of this component. If it is assumed that in the empty tunnel these quantities are sensibly uniform in any vertical plane in the neighborhood of the region to be occupied by the body, the flow as viewed in the plane

will depend only on  $\alpha + \alpha_s$  and  $\frac{d(\alpha + \alpha_s)}{dx}$  (where  $\alpha_s$  is the local stream angle) for the given body cross section in the plane. The stream angle will then cause an increment in the pressure coefficient at  $P$  which, to the order of the accuracy of the foregoing assumptions, is additive to the pressure coefficient for the empty tunnel. If the point  $P$  now moves to the body and the shielding effect is still neglected, the pressure coefficients as measured in the empty tunnel and those due to stream angle both act on the body and produce corrections to the aerodynamic coefficients.

Vertical pressure gradients.— The increments in lift and pitching-moment coefficients due to the vertical pressure gradients of the empty tunnel,  $\Delta C_{L_n}$  and  $\Delta C_{m_n}$ , respectively, may readily be calculated. The increment in lift coefficient with the base area as reference area is

$$C_{L_n} = \frac{2}{\pi a_b^2} \int_0^l dx \int_0^\pi \left( \frac{\Delta p_r}{q} \right) a \cos \theta d\theta \quad (A4)$$

where  $\Delta p_r/q$  is the ratio of the difference between the static pressure at the position of the body surface in the empty tunnel and the reference-wall static pressure to the free-stream dynamic pressure, and  $\theta$  is the angular position of the body meridian measured from the lower intersection of the vertical plane of symmetry with the body. The increment in moment coefficient, taking the moment about the body nose and using the body length as the reference length, is

$$\Delta C_{m_n} = \frac{2}{\pi a_b^2 l} \int_0^l x dx \int_0^\pi \left( \frac{\Delta p_r}{q} \right) a \cos \theta d\theta \quad (A5)$$

The fact that vertical pressure gradients may have a large effect on the aerodynamic coefficients of a slender body is associated with the inherent inefficiency of a slender body as a lifting device.

Stream angle.— For the body alone, the velocity potential given in reference 1 (with the velocity potential for uniform flow normal to the horizontal plane of symmetry subtracted out) reduces to

$$\phi = V_0 \alpha_s \sqrt{a^2 - y^2} \quad (A6)$$

When equation (A6) is substituted in equation (A3), the loading coefficient due to the stream-angle gradient becomes

$$\frac{\Delta p}{q} = 4 \frac{d\alpha_s}{dx} \sqrt{a^2 - y^2} \quad (A7)$$

Equation (A7) can be substituted in equation (A2) to give the lift due to stream-angle gradient on a spanwise strip of width  $dx$  as

$$\frac{d}{dx} \left( \frac{L}{q} \right) = 2\pi \alpha_s^2 \frac{d\alpha_s}{dx} \quad (A8)$$

The incremental spanwise lift due to the magnitude of the stream angle can be found, by substituting equation (A1) in equation (A2), to be

$$\frac{d}{dx} \left( \frac{L}{q} \right) = 4\pi \alpha_s a \frac{da}{dx} \quad (A9)$$

The addition of equation (A8) and equation (A9) yields the total-incremental spanwise lift due to stream angle as

$$\frac{d}{dx} \left( \frac{L}{q} \right)_s = 2\pi \frac{d}{dx} (a^2 \alpha_s) \quad (A10)$$

When equation (A10) is integrated over the body length and converted to coefficient form, the increment in lift coefficient due to stream angle becomes

$$\Delta C_{L_S} = \frac{2}{a_b^2} \int_0^{x_b} \frac{d}{dx} (a^2 \alpha_s) dx \quad (A11)$$

or

$$\Delta C_{L_S} = 2 \alpha_{S_b} \quad (A12)$$

Equation (A12) expresses the interesting result that the increment in lift coefficient due to stream angle for a pointed body of revolution depends only on the value of the stream angle at its base.

The increment in pitching-moment coefficient due to stream angle is

$$\Delta C_{m_S} = -\frac{2}{a_b^2 l} \left( a_b^2 l \alpha_{S_b} - \int_0^{x_b} a^2 \alpha_s dx \right) \quad (A13)$$

Cross-flow separation due to stream angle.— The experimental data can be corrected for the effect of cross-flow separation due to stream angle by the method of reference 9. When  $\alpha$  is replaced by  $\alpha + \alpha_s$ , reference 9 gives the force per unit length due to cross-flow separation as

$$f_v = 2\eta a c_{d_c} q \sin^2 (\alpha + \alpha_s) \quad (A14)$$

For small angles of attack, the cross force is nearly all lift and the net cross force can be determined approximately by integrating  $f_v$  over the body length. By conversion to coefficient form, there is obtained

$$C_{L_v} = \frac{A_p}{\pi a_b^2} \eta c_{d_c} \int_0^{x_b} \frac{\alpha + \alpha_s}{|\alpha + \alpha_s|} (\alpha + \alpha_s)^2 dx$$

For small angles of attack, the part of  $C_{L_v}$  due to stream angle is

$$\Delta C_{L_v} = \frac{2A_p}{\pi a_b^2} \eta c_{d_c} |\alpha| \int_0^{x_b} \alpha_s dx + \frac{A_p}{\pi a_b^2} \eta c_{d_c} \int_0^{x_b} \frac{\alpha_s}{|\alpha_s|} \alpha_s^2 dx \quad (A15)$$

The correction  $\Delta C_{L_v}$  increases with angle of attack. At large angles of attack,  $\alpha_s$  is usually small compared to  $\alpha$  so that in this case the second integral can be neglected.

The increment in pitching-moment coefficient due to the effect of stream angle on cross-flow separation is

$$\Delta C_{m_v} = - \frac{2A_p}{\pi a_b^2 l} \eta |\alpha| c_{d_c} \int_0^{x_b} x \alpha_s dx - \frac{A_p}{\pi a_b^2 l} \eta c_{d_c} \int_0^{x_b} x \frac{\alpha_s}{|\alpha_s|} \alpha_s^2 dx \quad (A16)$$

where moments are taken about the nose and the body length is the reference length.

Experimental verification.— Body-alone corrections obtained by the foregoing method have been compared with experimental pressure distributions obtained on a parabolic-arc body of revolution set at zero angle of attack in the 1- by 3-foot supersonic wind tunnel No. 2. The contour of the body is shown in figure 15. Stream angle and pressure surveys were made in the vertical plane of symmetry with the wind tunnel empty. The model was equipped with pressure orifices at a number of longitudinal stations and pressure measurements were made by rotating the body one revolution by increments of 30°. The increment in lift coefficient per unit body length  $\frac{d}{dx} (\Delta C_L)$  was determined from the pressure measurements. This distribution of  $\frac{d}{dx} (\Delta C_L)$  includes the combined effects of vertical pressure gradient, stream angle, and the effects of stream angle on cross-flow separation and is represented by squares in figure 15. However, the effect of cross-flow separation due to stream angle is negligible at zero angle of attack, so that, if the pressure measurements are corrected by subtracting out the pressures in the empty tunnel, the resulting distribution of  $\frac{d}{dx} (\Delta C_{L_s})$  should represent that due to stream angle alone. This corrected distribution is represented by the circles of figure 15. By the method already given, it is possible to predict the distribution of  $\frac{d}{dx} (\Delta C_{L_s})$  from the measured distribution of stream angle along the body. The predicted distribution is shown in figure 15 and is in fair agreement with the measured distribution corrected for vertical pressure gradients. From the figure, it is apparent that the effect of vertical pressure gradients and stream angle are of approximately equal magnitude.

#### Triangular Wing Corrections

The only corrections applied to the aerodynamic coefficients of the triangular wings were increments  $\Delta C_{L_s}$  and  $\Delta C_{m_s}$  to account for stream angle. For the wing alone, the velocity potential given in reference 1 reduces to

$$\phi = V_0 \alpha_s \sqrt{s^2 - y^2} \quad (A17)$$

When equation (A17) is substituted in equation (A3), the loading coefficient due to stream-angle gradient becomes

$$\left(\frac{\Delta p}{q}\right) = 4 \frac{d\alpha_s}{dx} \sqrt{s^2 - y^2} \quad (A18)$$

The lift on a spanwise strip of width  $dx$  is found from equation (A2) to be

$$\frac{d}{dx} \left(\frac{L}{q}\right) = 2\pi s^2 \frac{d\alpha_s}{dx} \quad (A19)$$

The incremental spanwise lift due to the magnitude of the stream angle can be found by substituting equation (A1) in equation (A2). The result is

$$\frac{d}{dx} \left(\frac{L}{q}\right) = 4\pi\alpha_s s \frac{ds}{dx} \quad (A20)$$

The addition of equations (A19) and (A20) yields the total incremental spanwise lift due to stream angle as

$$\frac{d}{dx} \left(\frac{L}{q}\right)_s = 2\pi \frac{d}{dx} (s^2 \alpha_s) \quad (A21)$$

When equation (A21) is integrated over the wing apex chord and converted to coefficient form, the increment in lift coefficient due to stream angle becomes

$$\Delta C_{L_s} = \frac{2\pi}{c_r s_m} \int_0^{c_r} \frac{d}{dx} (\alpha_s s^2) dx \quad (A22)$$

or

$$\Delta C_{L_s} = 2\pi\alpha_{s_t} \tan \epsilon \quad (A23)$$

Since equation (A23) is a result of slender-wing theory, the factor  $\lambda$  (described in the section THEORETICAL CONSIDERATIONS) is used to extend the results to higher-aspect-ratio triangular wings. The resulting equation is

$$\Delta C_{L_s} = 2\pi\lambda\alpha_{s_t} \tan \epsilon \quad (A24)$$

The increment in pitching moment due to stream angle is

$$\Delta C_{m_B}' = -\frac{3\pi\lambda}{s_m c_r^2} \left( \alpha_{s_t} s_m^2 c_r - \int_0^{c_r} \alpha_s s^2 dx \right) \quad (A25)$$

with the moments taken about the wing apex. To transfer the moment increment to the centroid of the wing plan-form area, the following equation is used:

$$\Delta C_{m_B} = \Delta C_{m_B}' + \Delta C_{L_B} \quad (A26)$$

### Wing-Body Combination Corrections

The only corrections applied to the wing-body combinations were increments of lift and pitching-moment coefficient to account for stream angle. The corrections have been determined using a theory analogous to that used for the body and the wings. The wing-body combinations can be considered to consist of three parts: (1) from the nose of the body to the intersection of the wing leading edge and the body  $x_l$ , (2) from  $x_l$  to the wing trailing edge  $x_t$ , and (3) from  $x_t$  to the body base  $x_b$ . Over the first part of the combination the analysis is the same as that for the body alone, but the limits of integration are changed. For this part the increment in lift coefficient due to stream angle is given by

$$\Delta C_{L_B} = \frac{2\pi}{s_m c_r} \int_0^{x_l} \frac{d}{dx} (a^2 \alpha_s) dx \quad (A27)$$

For wing-body combinations similar to those of the present tests (in which the exposed wing lies entirely along the cylindrical part of the body), the velocity potential due to the body, for the second part, is given by

$$\Phi_B = V_0 \alpha_s \left[ \sqrt{(s^2 + a^2)^2 - 4y^2} - \sqrt{a^2 - y^2} \right] \quad (A28)$$

and the velocity potential for the wing is given by

$$\Phi_W = V_0 \alpha_s s \sqrt{\left(1 + \frac{s^4}{s^4}\right) - \frac{y^2}{s^2}} \left(1 + \frac{a^4}{s^4}\right) \quad (A29)$$

When equations (A28) and (A29) are substituted in equation (A3), the loading coefficients due to the stream-angle gradient become

$$\left(\frac{\Delta p}{q}\right)_B = 4 \frac{d\alpha_s}{dx} \left[ s \sqrt{\left(1 + \frac{a^2}{s^2}\right)^2 - 4 \frac{y^2}{s^2}} - \sqrt{a^2 - y^2} \right] \quad (A30)$$

and

$$\left(\frac{\Delta p}{q}\right)_W = 4 \frac{d\alpha_s}{dx} s \sqrt{\left[1 + \frac{a^4}{s^4} - \frac{y^2}{s^2} \left(1 + \frac{a^4}{s^4}\right)\right]} \quad (A31)$$

The lift on a spanwise strip of width  $dx$  due to the gradient in stream angle is found from equation (A2) to be

$$\frac{d}{dx} \left(\frac{L}{q}\right) = 2\pi \frac{d\alpha_s}{dx} s^2 \left(1 - \frac{a^2}{s^2} + \frac{a^4}{s^4}\right) \quad (A32)$$

The incremental spanwise lift due to the magnitude of the stream angle can be found by substituting equation (A1) in equation (A2). The result is

$$\frac{d}{dx} \left(\frac{L}{q}\right)_s = 2\pi \frac{d}{dx} \left[ \alpha_s s^2 \left(1 - \frac{a^2}{s^2} + \frac{a^4}{s^4}\right) \right] dx \quad (A33)$$

Thus the increment in lift coefficient due to stream angle for the second part is given by

$$\Delta C_{L_s} = \frac{2\pi}{s_m c_r} \int_{x_l}^{x_t} \frac{d}{dx} \left[ \alpha_s s^2 \left(1 - \frac{a^2}{s^2} + \frac{a^4}{s^4}\right) \right] dx \quad (A34)$$

For the third part, the analysis is again the same as that for the body alone, with the limits of integration changed. When this part of the body is cylindrical, as in the present case, the effect of the magnitude of the stream angle is zero, and the incremental spanwise lift due to stream angle is that due to gradient of stream angle. This is given by

$$\frac{d}{dx} \left(\frac{L}{q}\right) = 2\pi a_b^2 \frac{d\alpha_s}{dx} \quad (A35)$$

The increment in lift coefficient due to stream angle for the third part is

$$\Delta C_{L_s} = 2\pi a_b^2 \int_{x_t}^{x_b} \frac{d\alpha_s}{dx} dx \quad (A36)$$

The increment in lift coefficient for the combination is then found (by integrating over the three parts of the configuration and applying the factor  $\lambda$  to the second part) to be

$$\Delta C_{L_S} = \frac{2\pi a_b^2}{s_m c_r} \alpha_{S_L} + \frac{2\pi\lambda}{s_m c_r} \left[ s_m^2 \left( 1 - \frac{a_b^2}{s_m^2} + \frac{a_b^2}{s_m^4} \right) \alpha_t - a_b^2 \alpha_{S_L} \right] + \frac{2\pi}{s_m c_r} a_b^2 (\alpha_{S_b} - \alpha_{S_t}) \quad (A37)$$

The corresponding increment in pitching-moment coefficient about the body nose is

$$\Delta C_{m_S}' = -\frac{3\pi}{s_m c_r^2} \int_0^{x_L} x \frac{d}{dx} (a^2 \alpha_S) dx - \frac{3\pi\lambda}{s_m c_r^2} \int_{x_L}^{x_t} x \frac{d}{dx} \left[ s^2 \left( 1 - \frac{a^2}{s^2} + \frac{a^4}{s^4} \right) \alpha_S \right] dx - \frac{3\pi a_b^2}{s_m c_r^2} \int_{x_t}^{x_b} \frac{d}{dx} (\alpha_S) dx \quad (A38)$$

The increment in moment coefficient transferred to the centroid of the wing plan-form area is

$$\Delta C_{m_S} = \Delta C_{m_S}' + \frac{x_{WC}}{c} \Delta C_{L_S} \quad (A39)$$

where  $x_{WC}$  is the distance from the body nose to the centroid of the wing plan-form area.

#### REFERENCES

1. Spreiter, John R.: Aerodynamic Properties of Slender Wing-Body Combinations at Subsonic, Transonic, and Supersonic Speeds. NACA TN 1662, 1948.
2. Ferrari, Carlo: Interference Between Wing and Body at Supersonic Speeds - Theory and Numerical Application. Jour. of Aero. Sci., vol. 15, no. 6, June 1948, pp. 317-336.
3. Browne, S. H., Friedman, L., and Hodes, I.: A Wing-Body Problem in Supersonic Conical Flow. North American Rept. AL-387, Nov. 13, 1947.

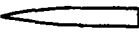
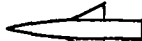
4. Van Dyke, Milton D.: Aerodynamic Characteristics Including Scale Effect of Several Wings and Bodies Alone and in Combination at a Mach Number of 1.53. NACA RM A6K22, 1946.
5. Vincenti, Walter G., Nielsen, Jack N., and Matteson, Frederick H.: Investigation of Wing Characteristics at a Mach Number of 1.53. I - Triangular Wings of Aspect Ratio 2. NACA RM A7I10, 1947.
6. Tsien, Hsue-Shen: Supersonic Flow Over an Inclined Body of Revolution. Jour. Aero. Sci., vol. 5, no. 12, Oct. 1938, pp. 480-483.
7. Munk, Max. M.: The Aerodynamic Forces on Airship Hulls. NACA Rep. 184, 1924.
8. Jones, Robert T.: Effects of Sweepback on Boundary Layer and Separation. NACA Rep. 884, 1947.
9. Allen, H. Julian: Estimation of the Forces and Moments Acting on Inclined Bodies of Revolution of High Fineness Ratio. NACA RM A9I26, 1949.
10. Brown, Clinton E.: Theoretical Lift and Drag of Thin Triangular Wings at Supersonic Speeds. NACA Rep. 839, 1946.
11. Stewart, H. J.: The Lift of a Delta Wing at Supersonic Speeds. Quart. of Applied Math., vol. IV, no. 3, Oct. 1946.
12. Puckett, Allen E.: Supersonic Wave Drag of Thin Airfoils. Jour. Aero. Sci., vol. 13, no. 9, Sept. 1946, pp. 475-484.
13. Jones, Robert T.: Properties of Low-Aspect-Ratio Pointed Wings at Speeds Below and Above the Speed of Sound. NACA Rep. 835, 1946.
14. Love, Eugene S.: Investigation at Supersonic Speeds of 22 Triangular Wings Representing Two Airfoil Sections for Each of 11 Apex Angles. NACA RM L9D07, 1949.

TABLE I.— SUMMARY OF GEOMETRICAL PROPERTIES OF WINGS

Wing	W <sub>1</sub>	W <sub>2</sub>	W <sub>3</sub>	W <sub>4</sub>	W <sub>5</sub>	W <sub>6</sub>
Sketch						
$\Lambda_0$ (deg)	80.4	71.6	63.2	56.0	50.3	45.0
$\Lambda_{\frac{1}{2}}$ (deg)	71.4	56.2	44.7	36.6	31.0	26.6
$s_m$ (in.)	1.25	1.75	2.25	2.76	3.24	3.74
$\bar{c}$ (in.)	4.95	3.49	2.97	2.73	2.60	2.49
$c_r$ (in.)	7.43	5.23	4.45	4.10	3.90	3.74
$S$ (in. <sup>2</sup> )	9.29	9.15	10.01	11.30	12.66	13.99
$A$	0.67	1.34	2.02	2.69	3.33	4.00



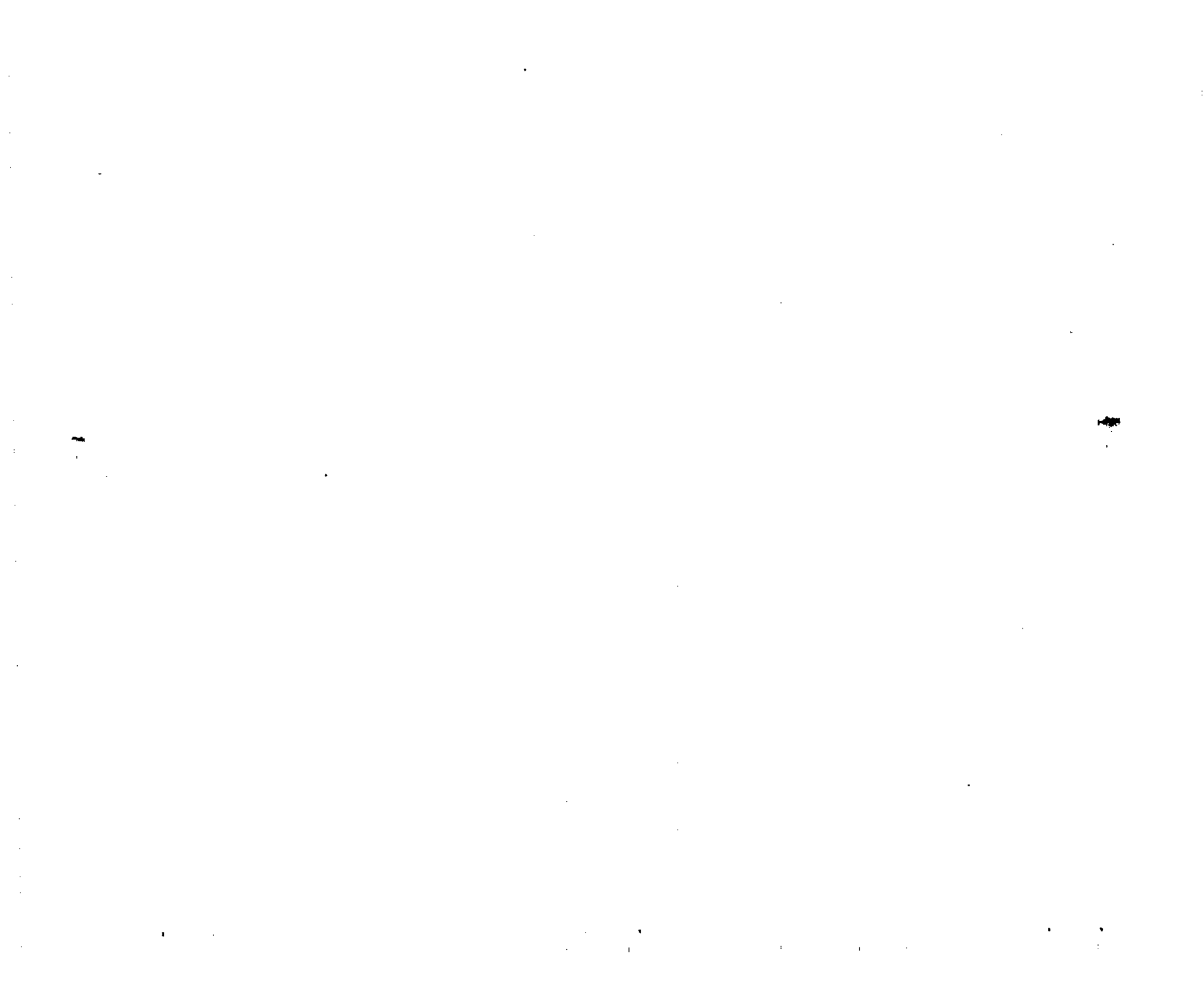
TABLE II.— SUMMARY OF RESULTS

Configuration		Lift		Moment	
Symbol	Sketch	$\left(\frac{dC_L}{d\alpha}\right)_{L \rightarrow 0}$ (per deg)		$\left(\frac{dC_m}{dC_L}\right)_{L \rightarrow 0}$	
		$M_0=1.50$	$M_0=2.02$	$M_0=1.50$	$M_0=2.02$
B		0.0340 (.0349)	0.0460 (.0349)	-0.20 (-.190)	-0.20 (-.190)
W <sub>1</sub>		.0208 (.0176)	.0186 (.0169)	-.09 (0)	-.03 (0)
W <sub>2</sub>		.0305 (.0323)	.0275 (.0289)	0 (0)	.06 (0)
W <sub>3</sub>		.0387 (.0442)	.0347 (.0374)	.03 (0)	.06 (0)
W <sub>4</sub>		.0455 (.0533)	.0395 (.0398)	.03 (0)	.04 (0)
W <sub>5</sub>		.0507 (.0602)	.0425 (.0398)	.06 (0)	.04 (0)
W <sub>6</sub>		.0544 (.0624)	.0416 (.0398)	.07 (0)	.08 (0)
W <sub>1</sub> B		.0160 (.0137)	.0163 (.0134)	.12 (.180)	.20 (.191)
W <sub>2</sub> B		.0300 (.0282)	.0275 (.0260)	.11 (.147)	.12 (.175)
W <sub>3</sub> B		.0405 (.0408)	.0373 (.0354)	.11 (.113)	.10 (.150)
W <sub>4</sub> B		.0473 (.0510)	.0415 (.0395)	.09 (.0941)	.08 (.148)
W <sub>5</sub> B		.0526 (.0590)	.0451 (.0405)	.06 (.0819)	.06 (.151)
W <sub>6</sub> B		.0571 (.0622)	.0460 (.0410)	.08 (.0798)	.08 (.150)

Note: In each case the experimental value is given first and the corresponding theoretical value indicated in parentheses directly below.







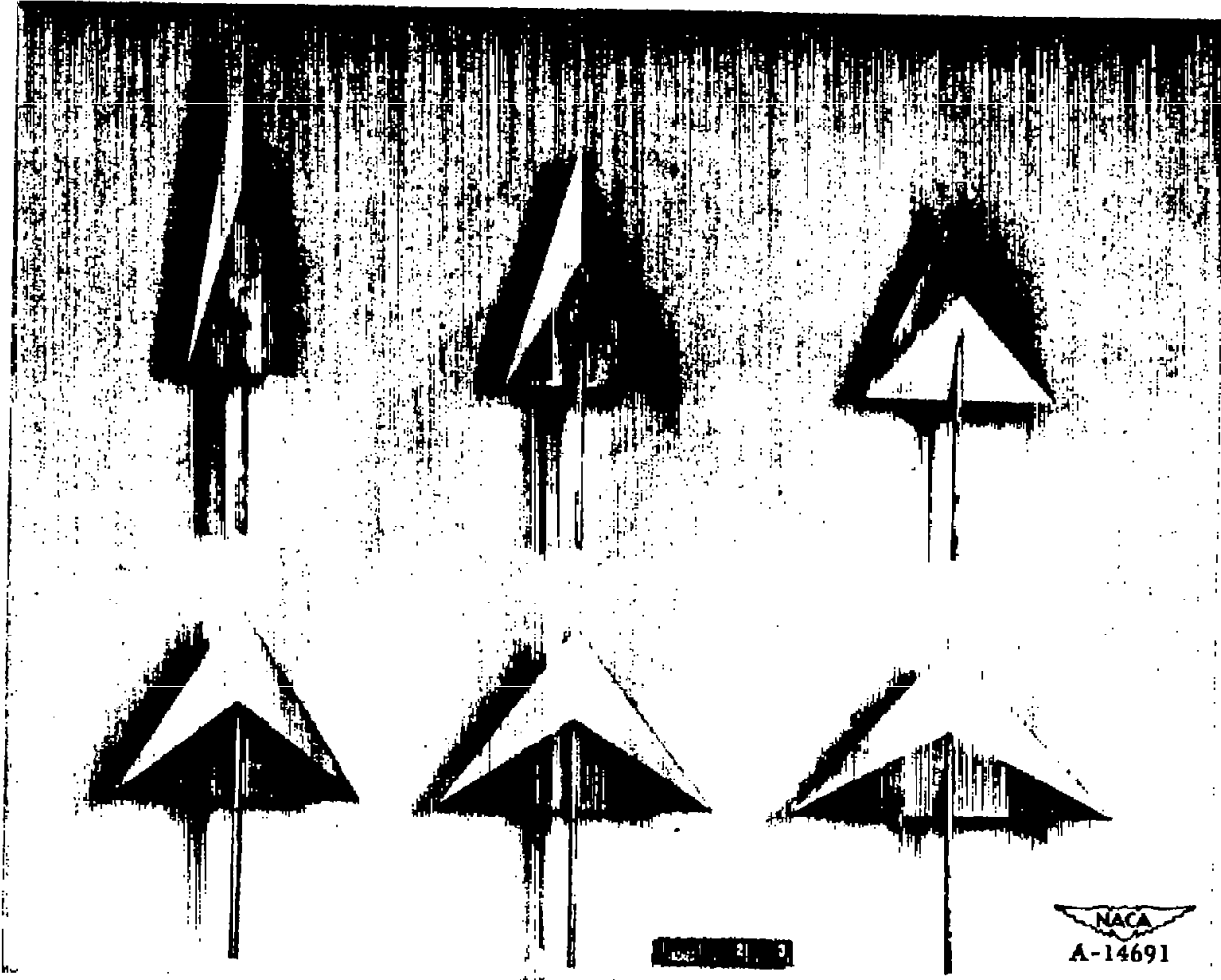
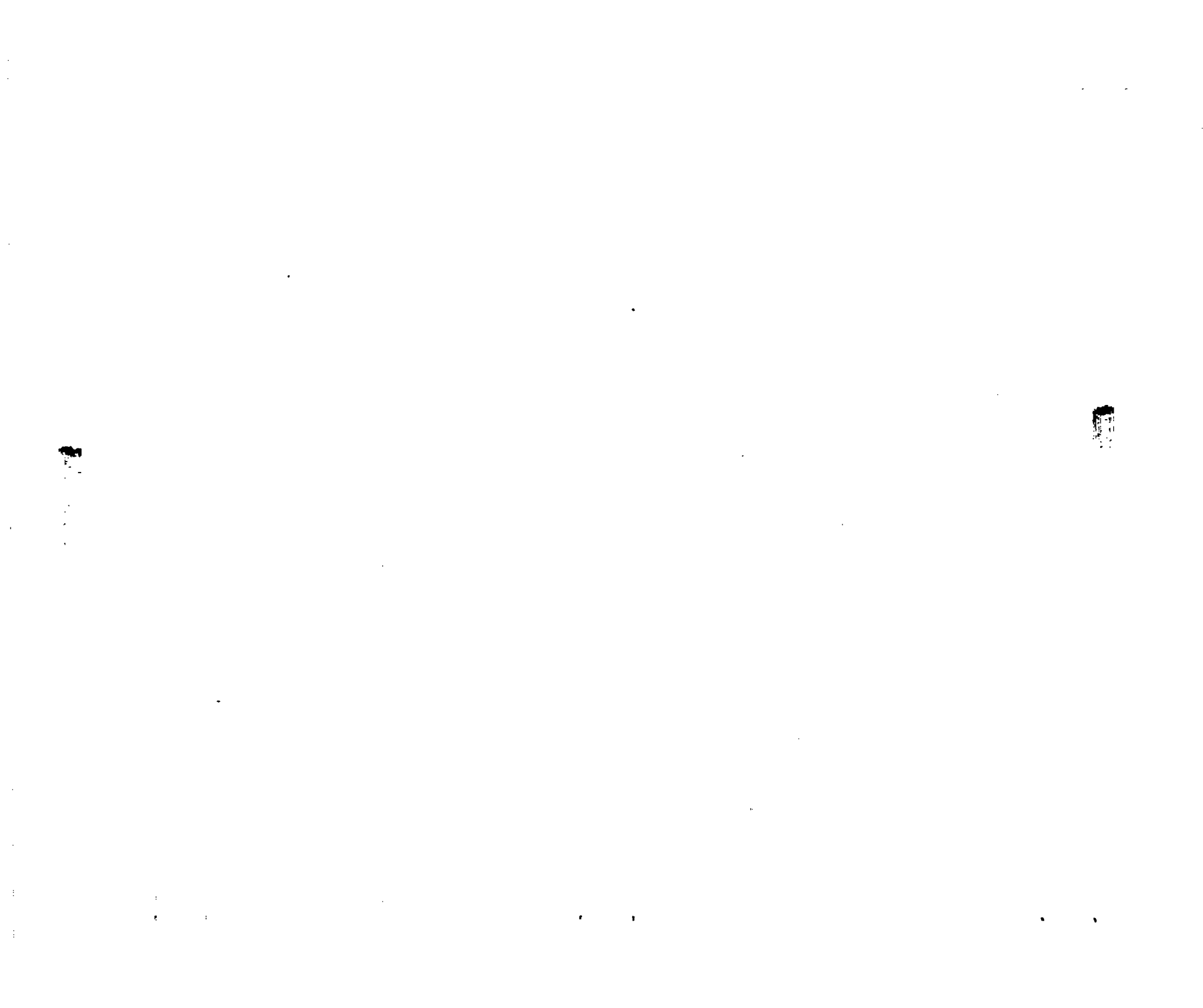


Figure 2.- Wing series.



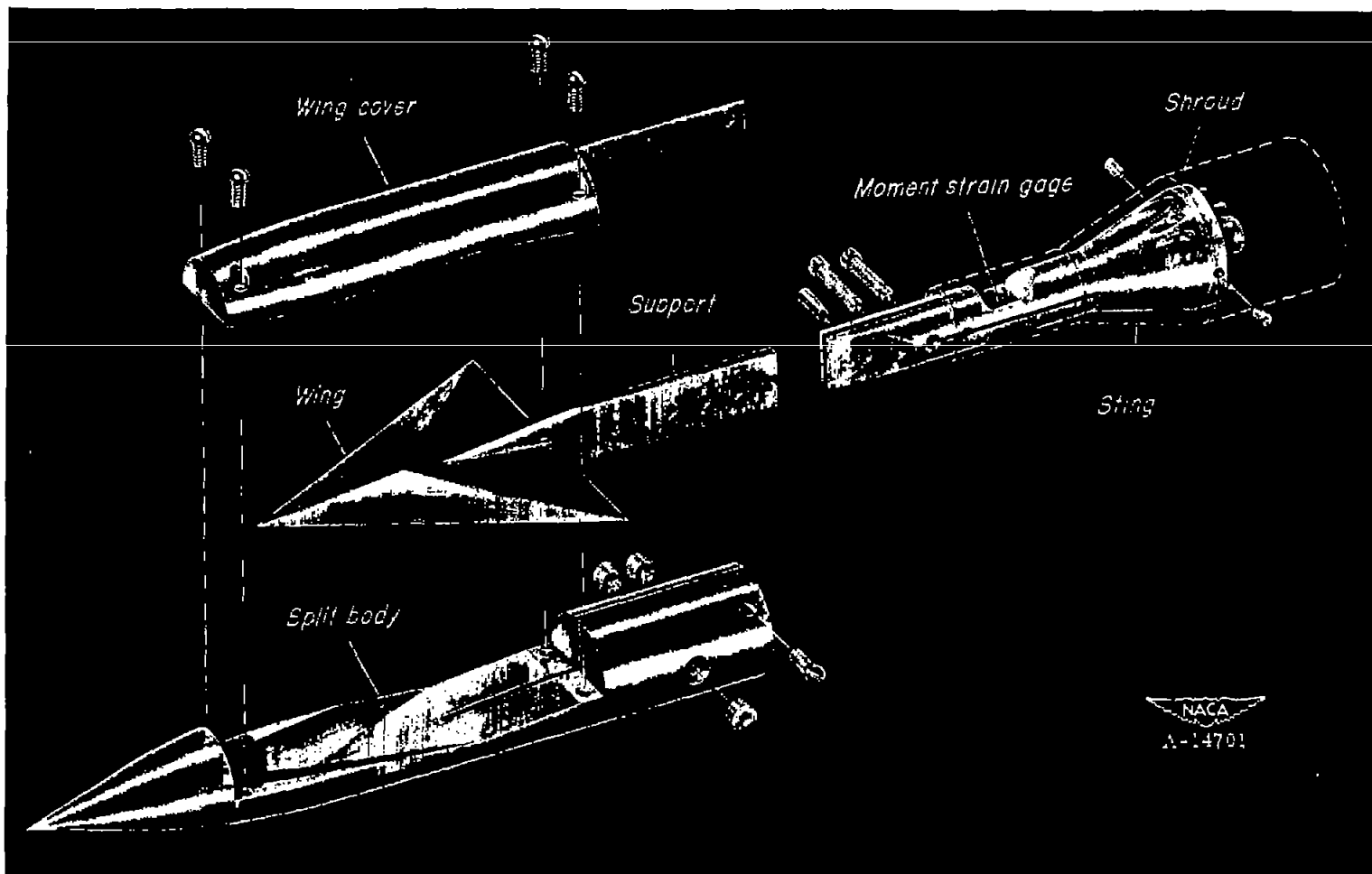


Figure 3.- Exploded view of body, wing, and sting.

1

2

3

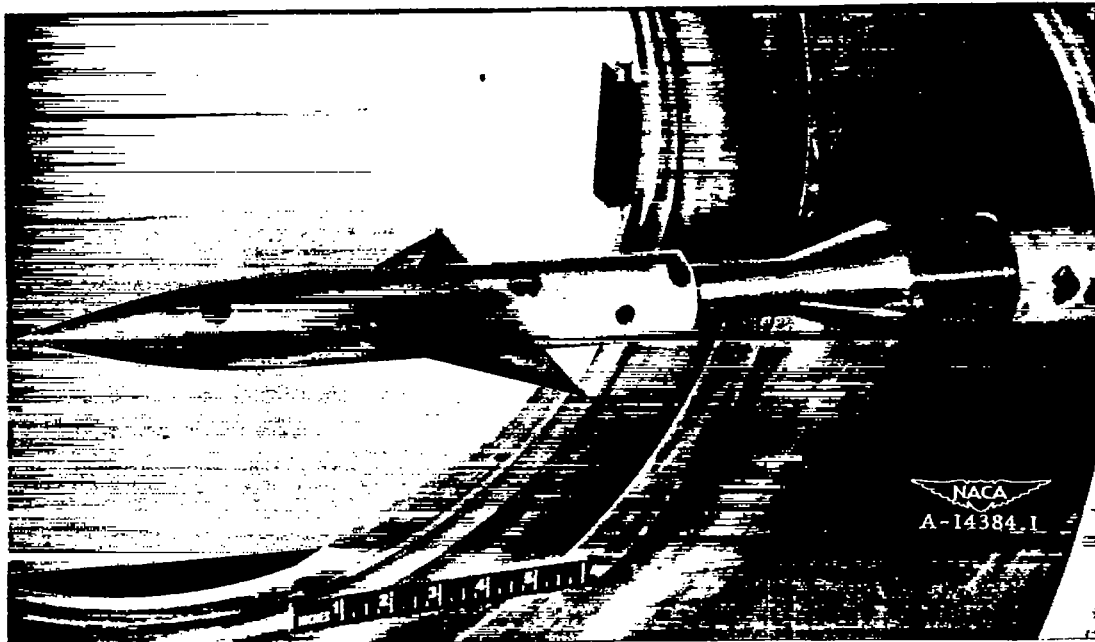
4

5

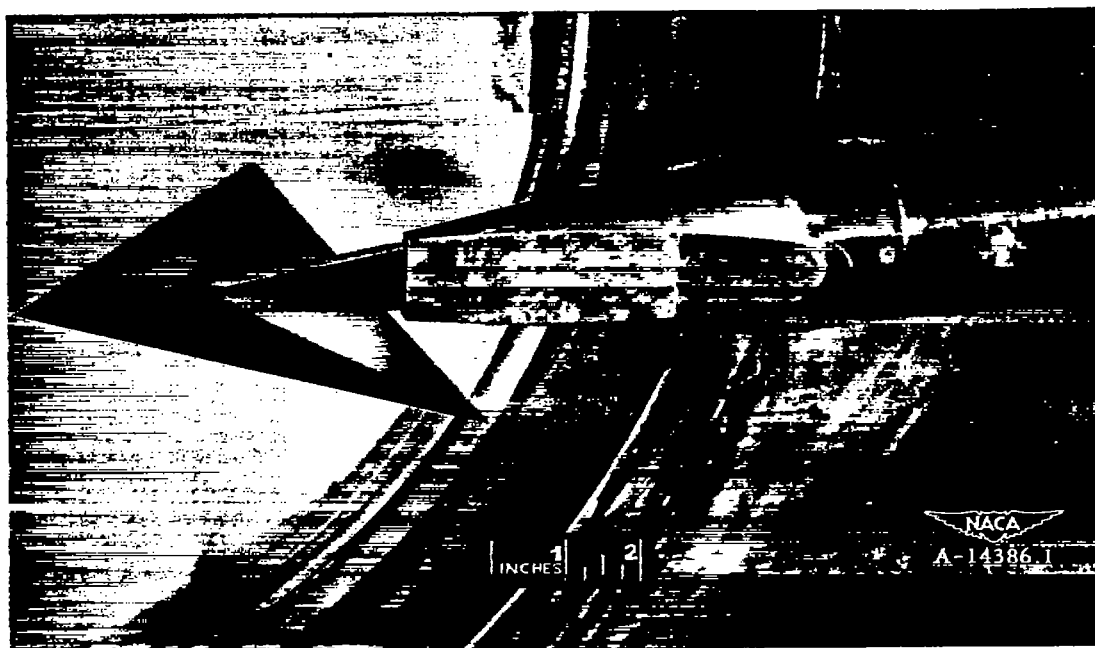
6

7

8

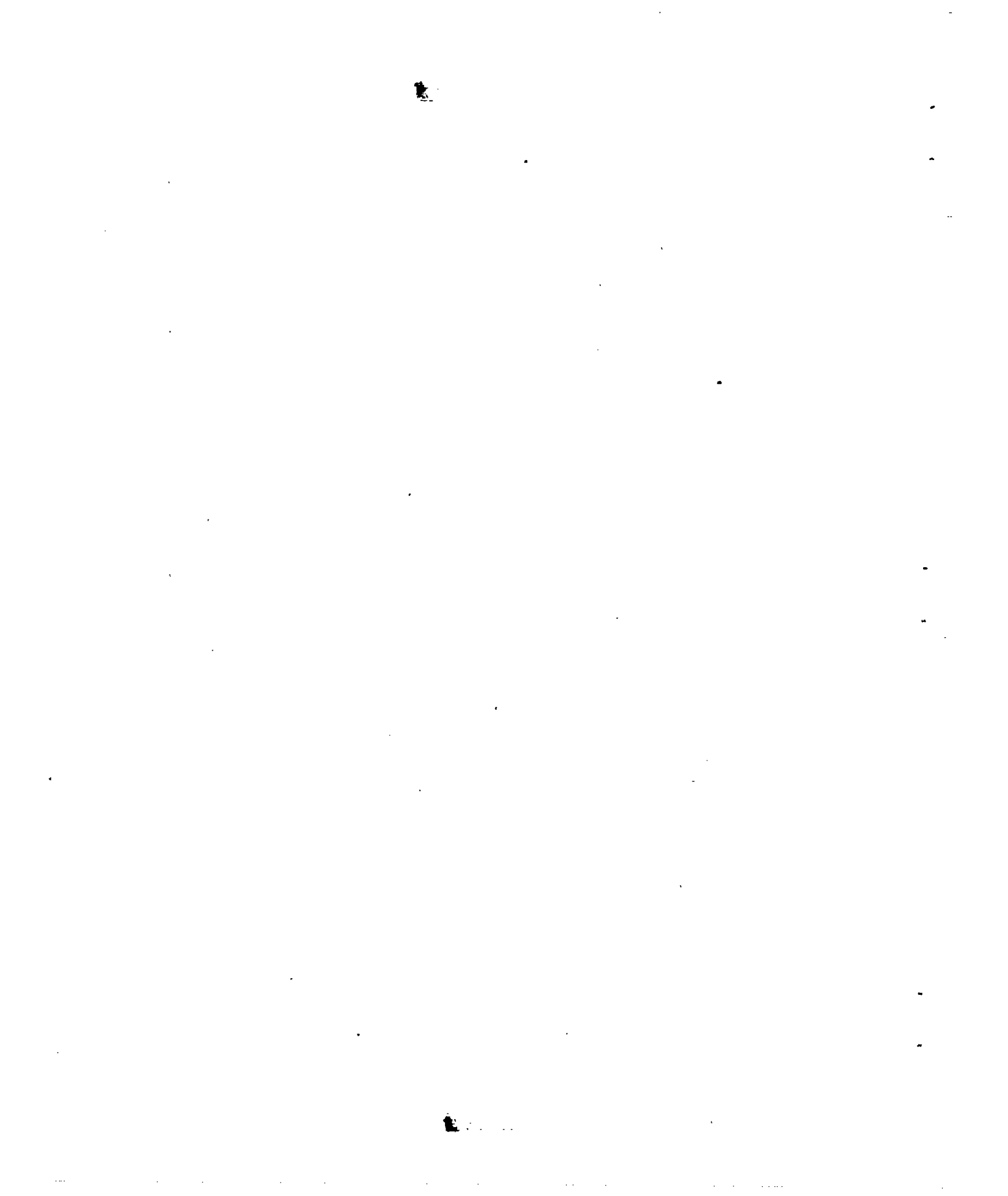


(a) Wing-body combination.



(b) Wing alone.

Figure 4.- Wing and wing-body combination mounted in tunnel.



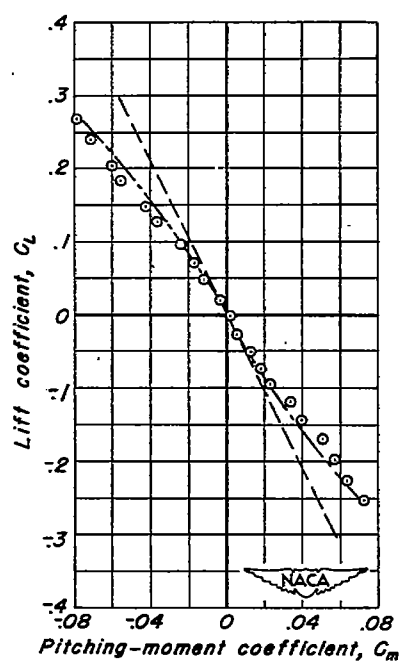
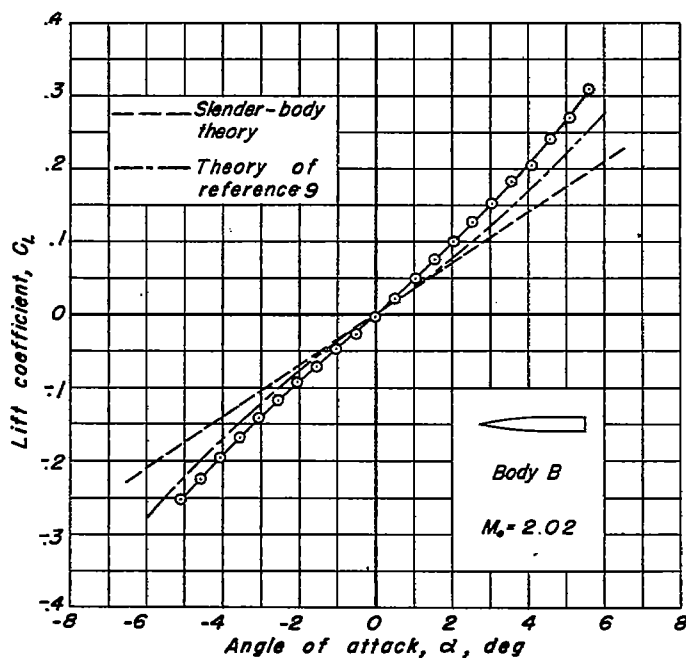
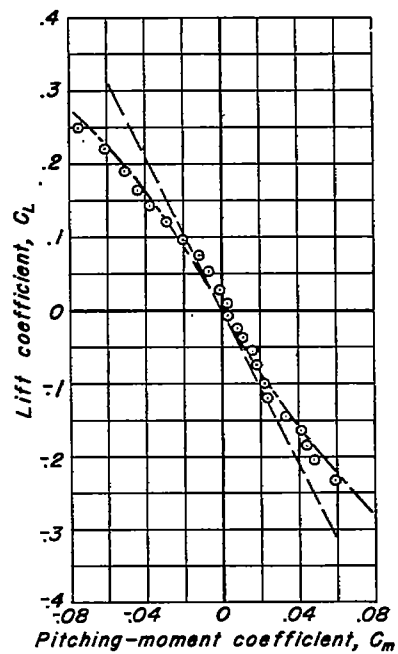
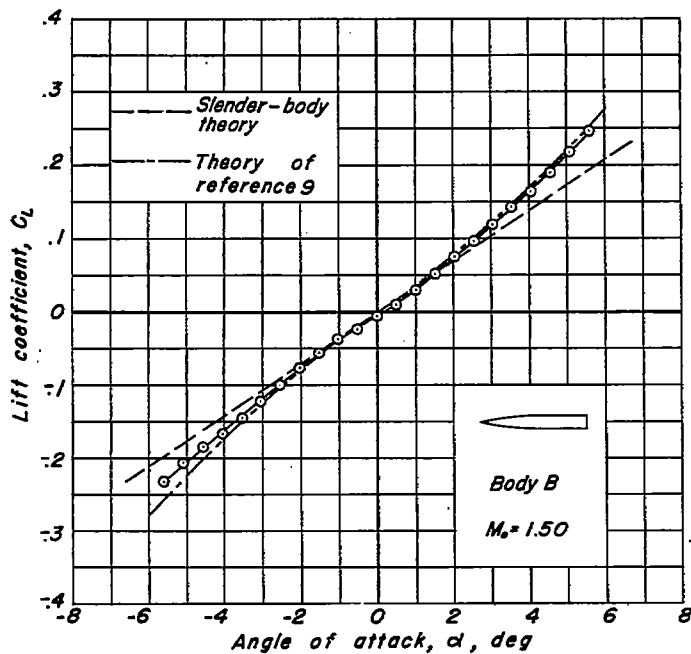
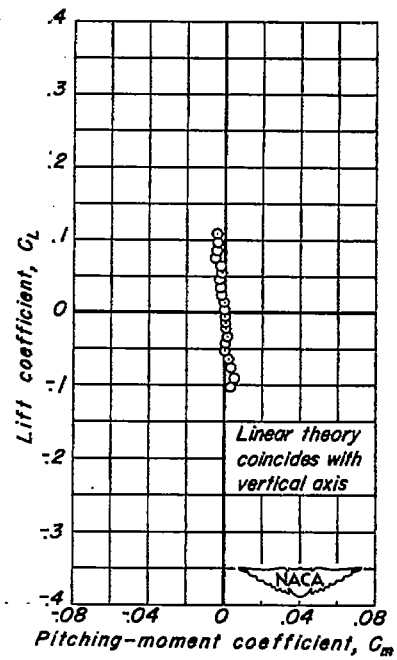
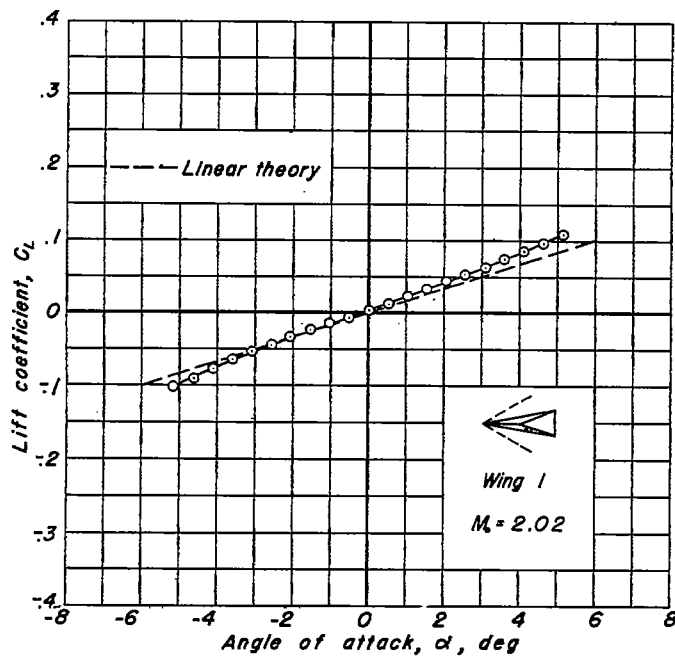
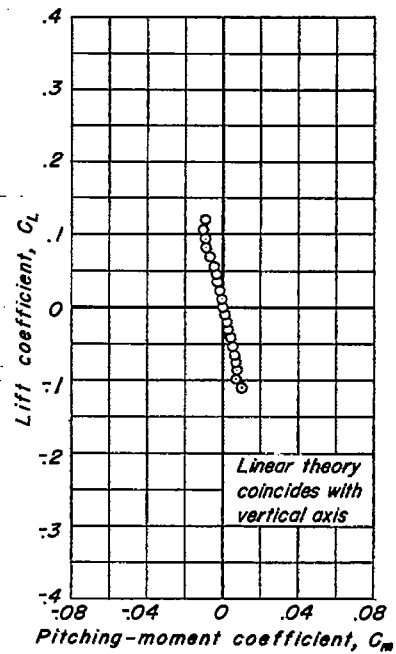
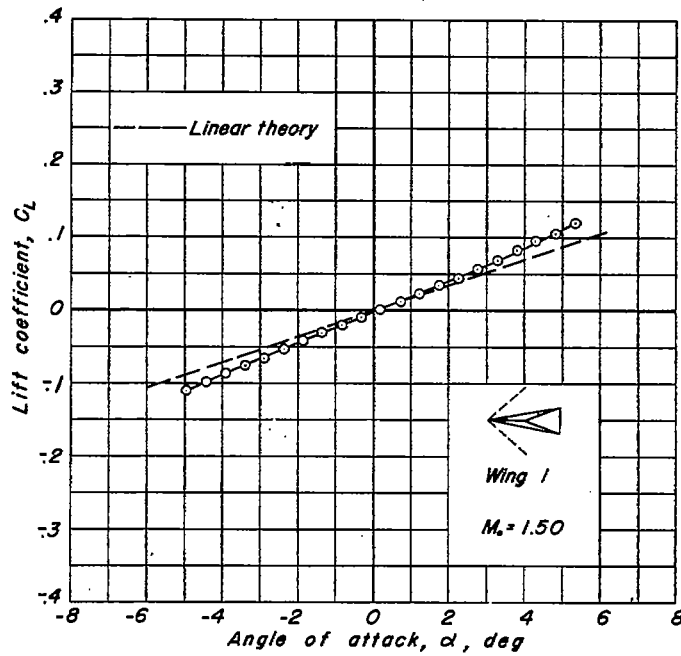
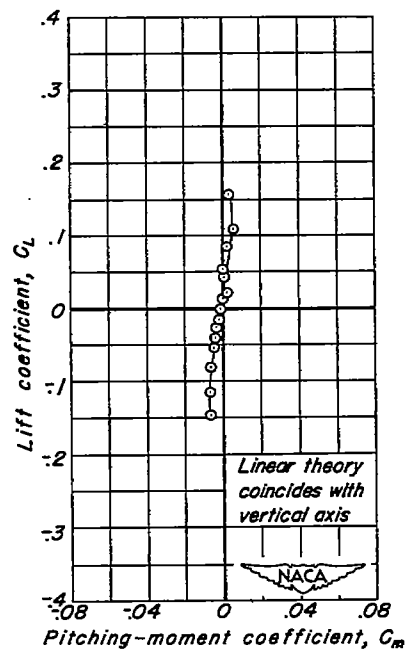
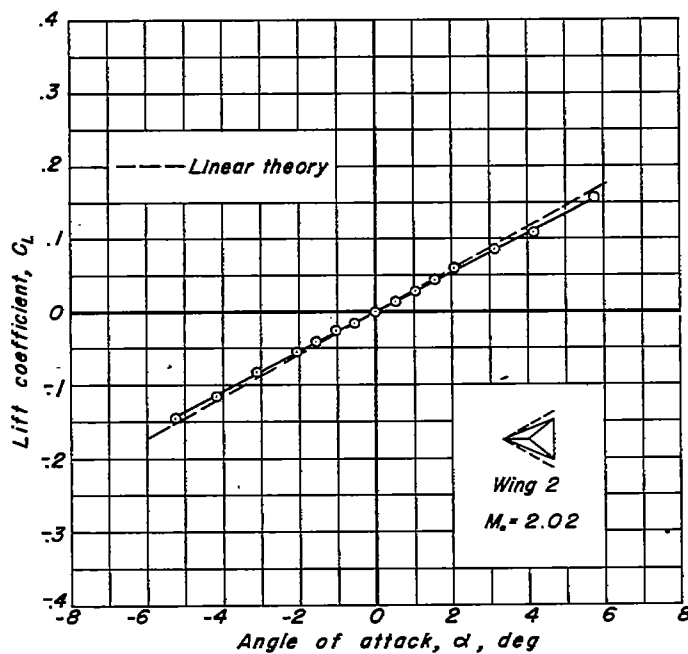
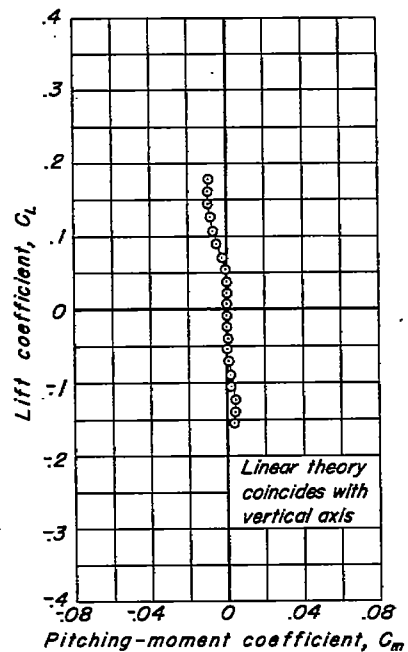
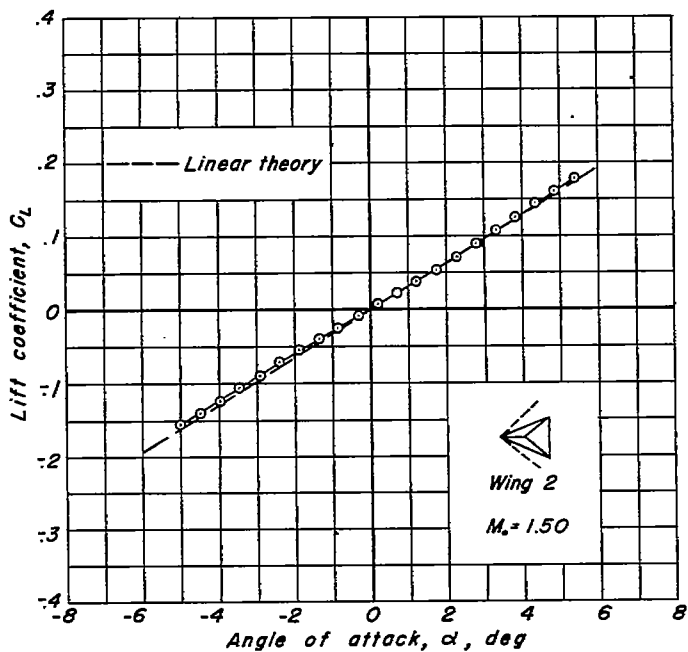


Figure 5.—Lift and moment coefficients for body at  $M_0 = 1.50$  and  $M_0 = 2.02$ .



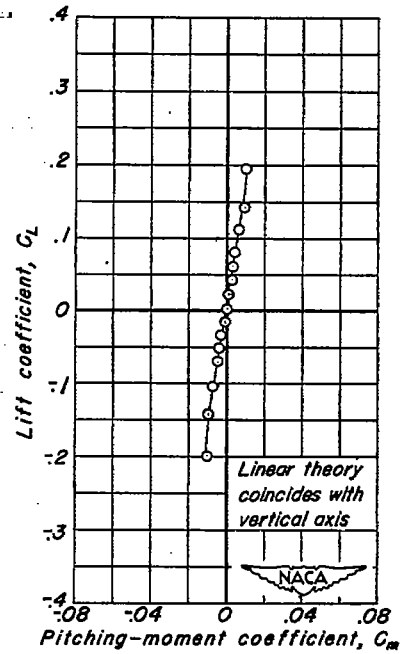
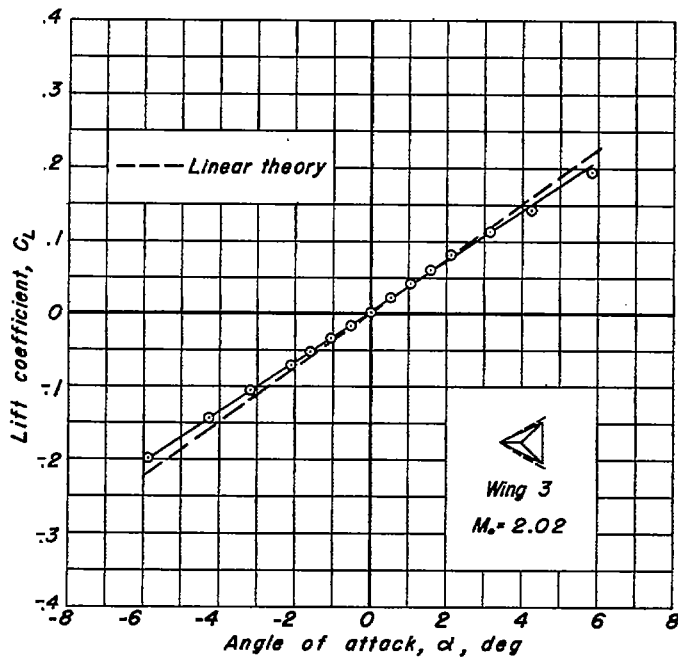
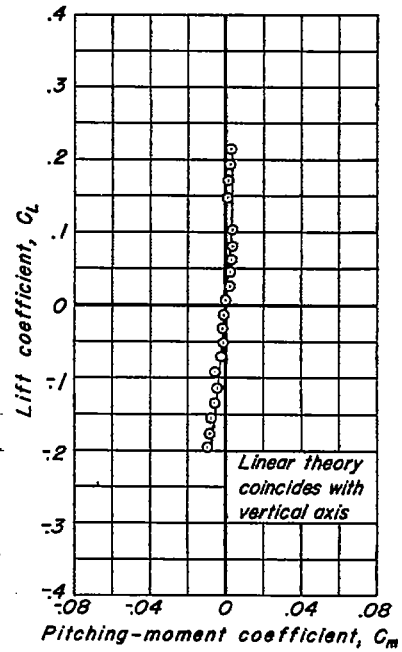
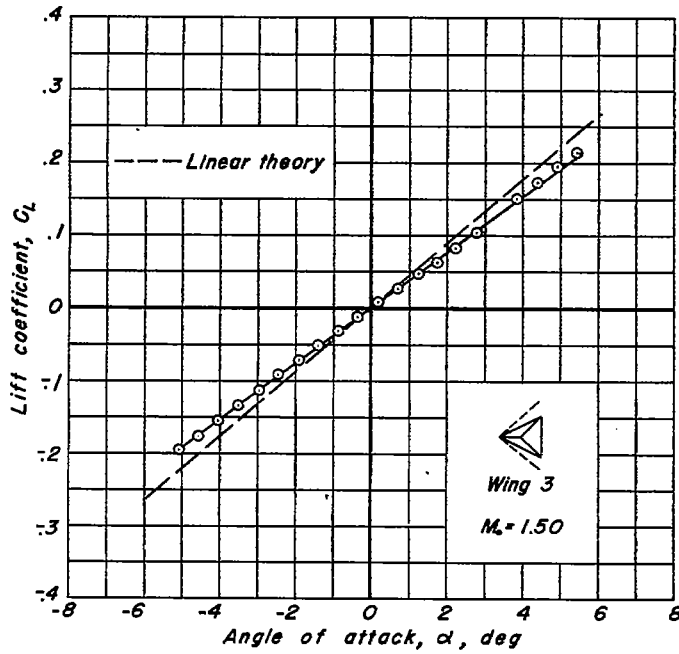
(a) Wing 1.

Figure 6 .— Lift and moment coefficients of wings at  $M_0 = 1.50$  and  $M_0 = 2.02$ .



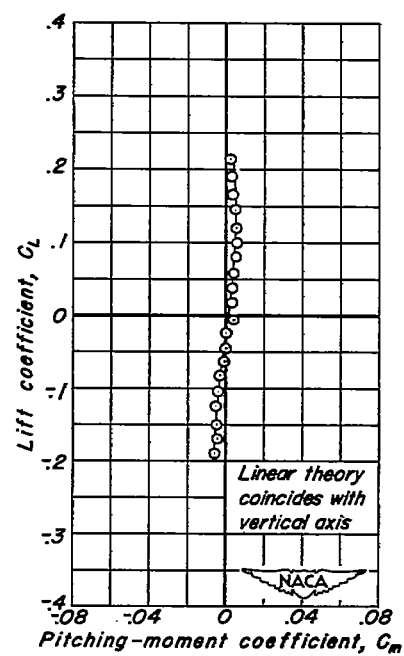
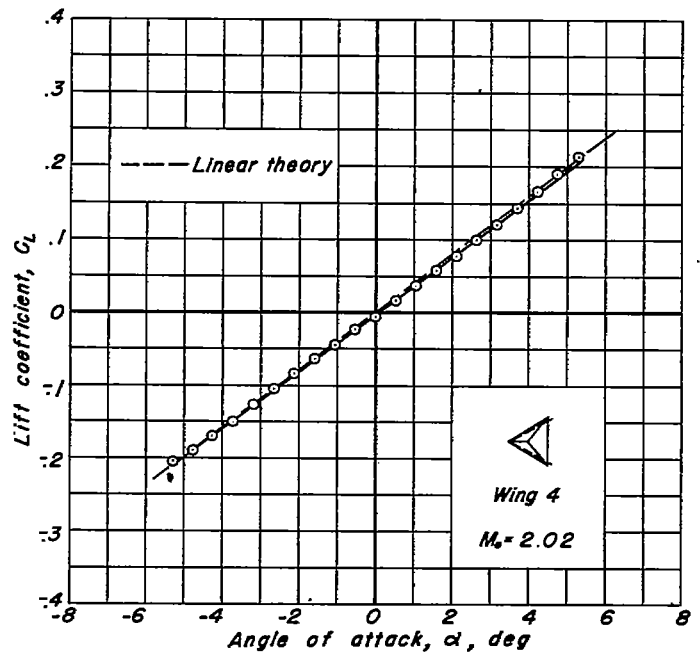
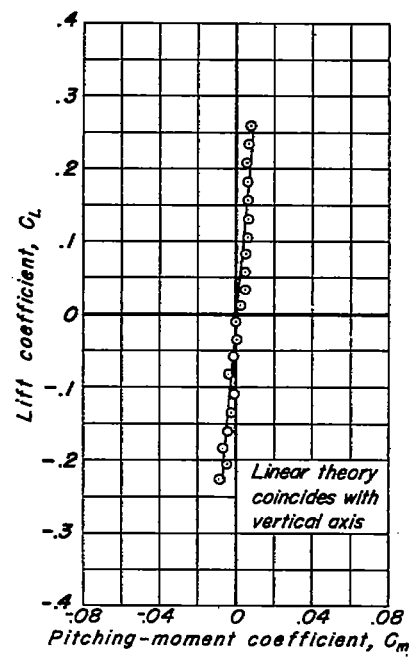
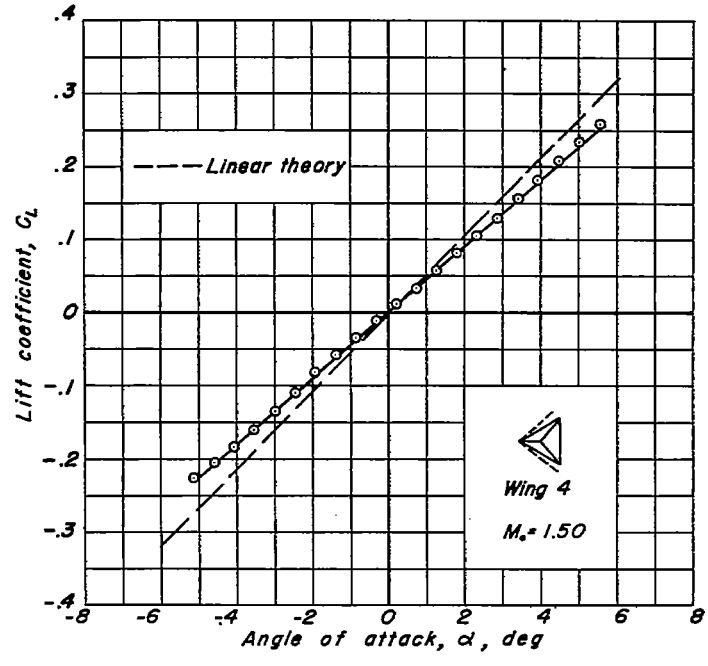
(b) Wing 2.

Figure 6.— Continued.



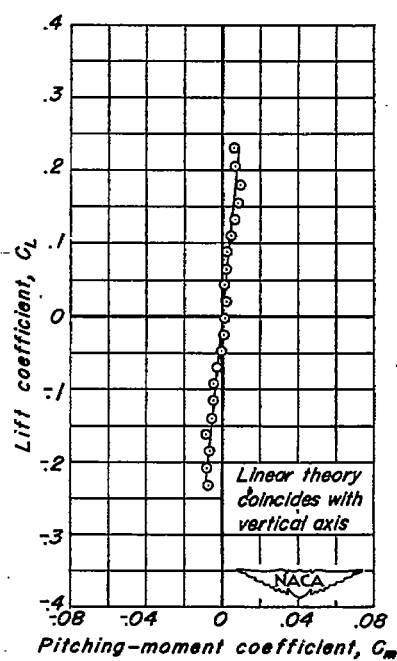
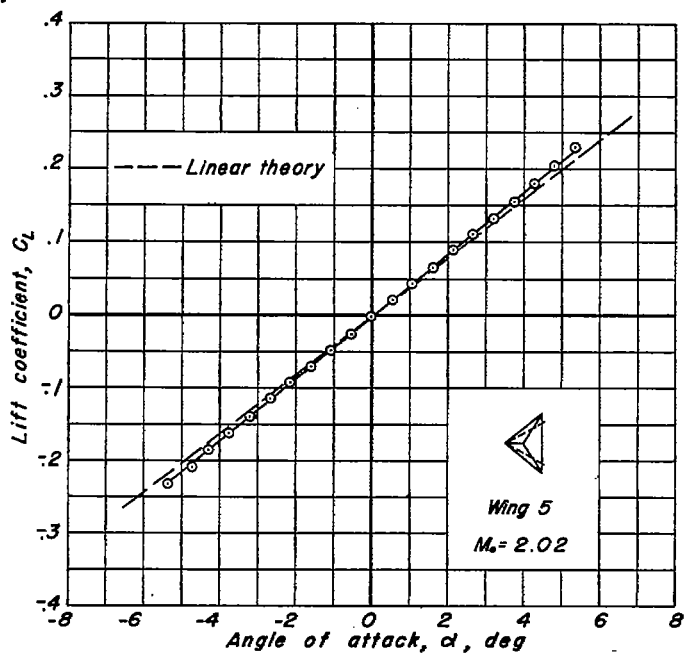
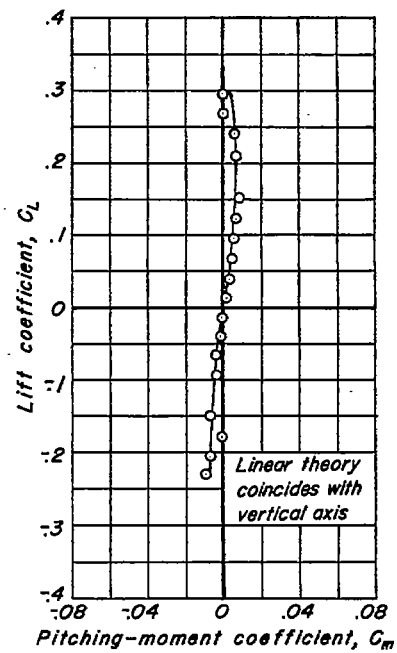
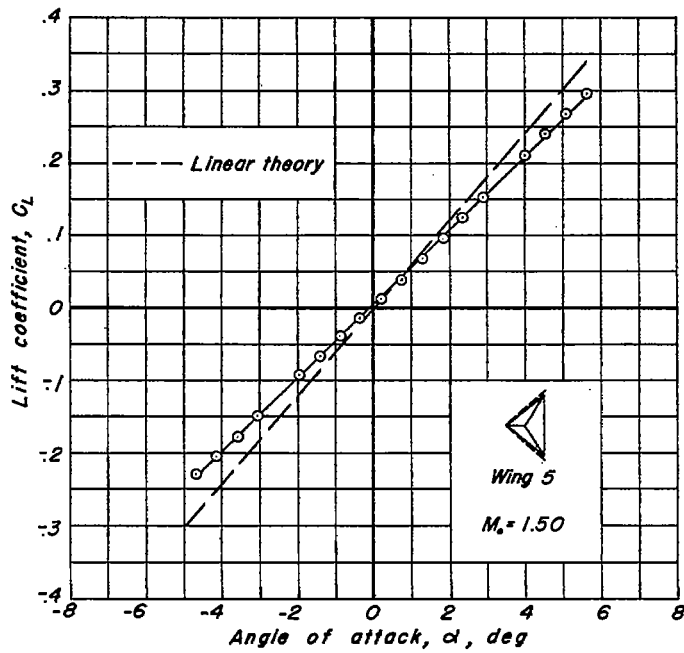
(c) Wing 3.

Figure 6.— Continued.



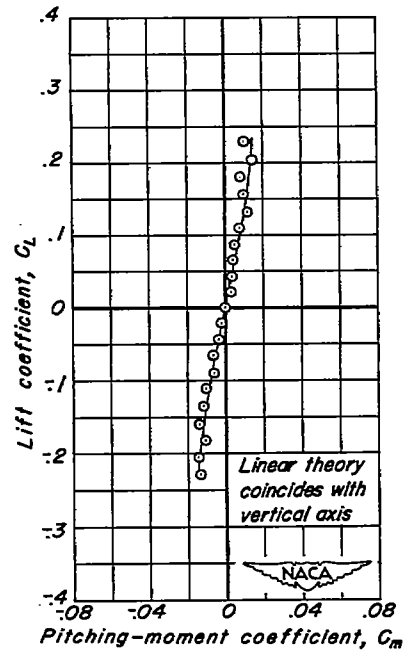
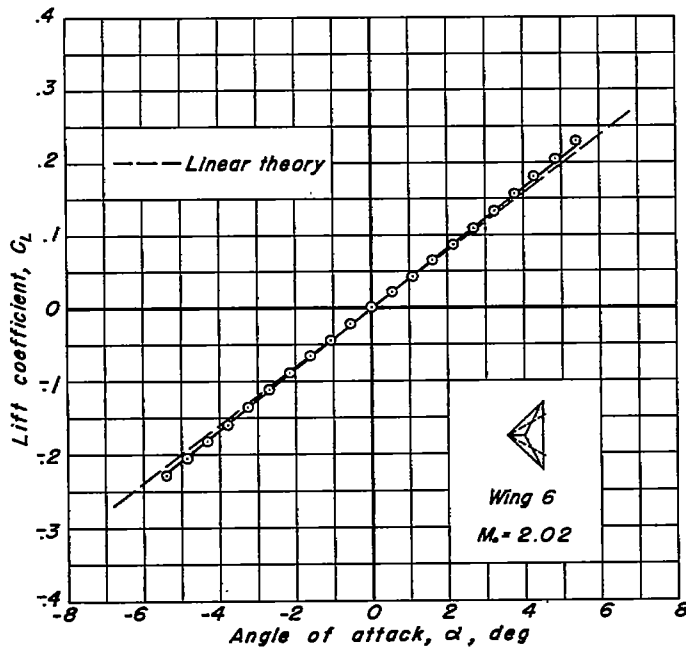
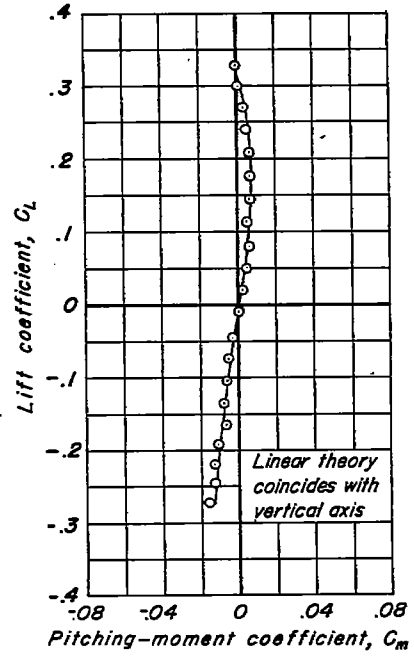
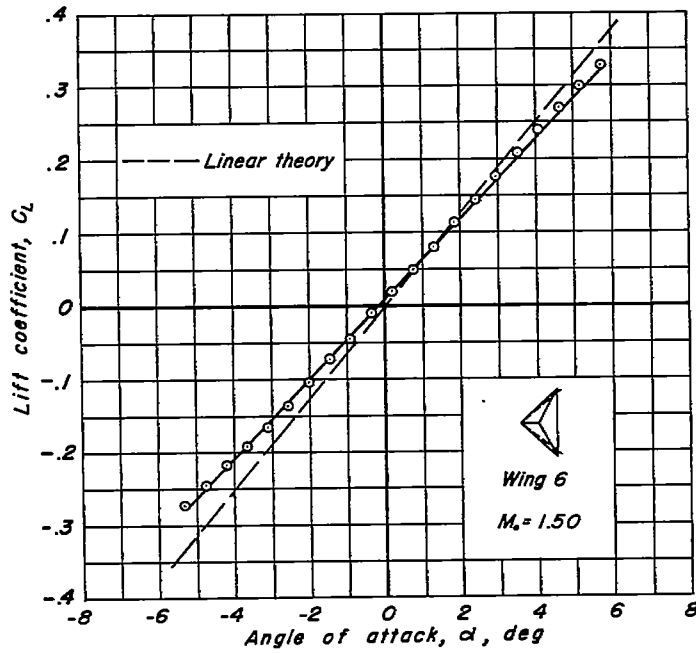
(d) Wing 4.

Figure 6.— Continued.



(e) Wing 5.

Figure 6. — Continued.



(f) Wing 6.

Figure 6. - Concluded.

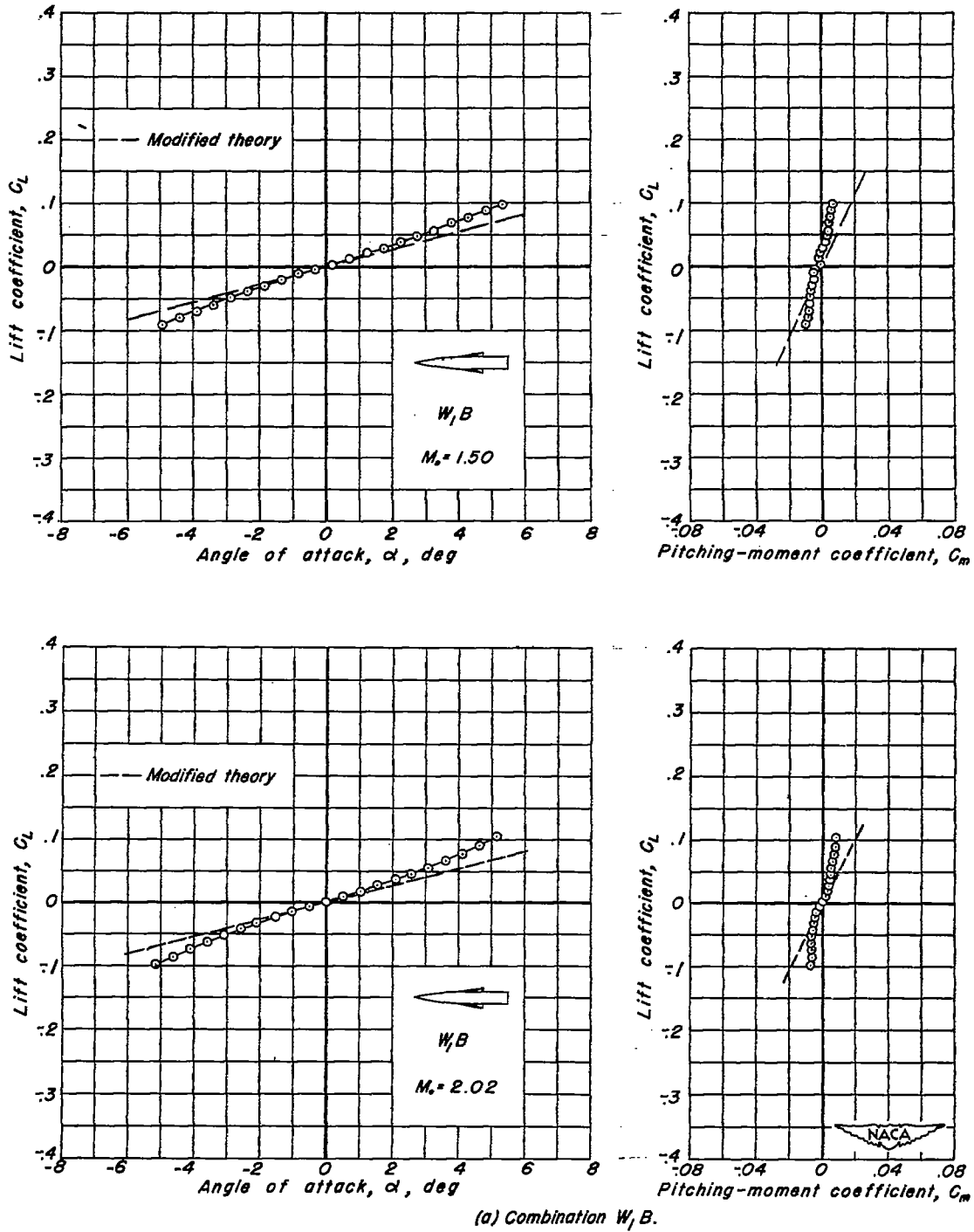
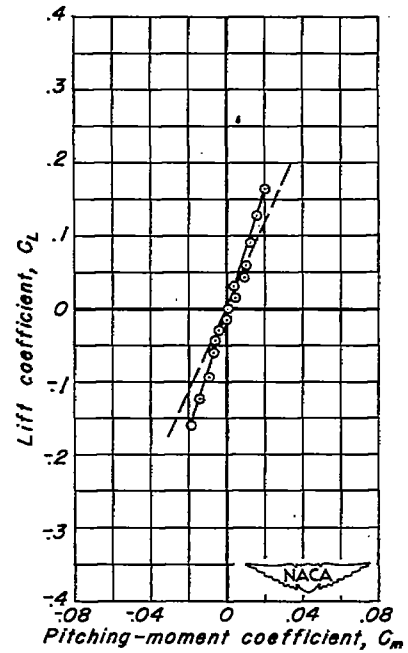
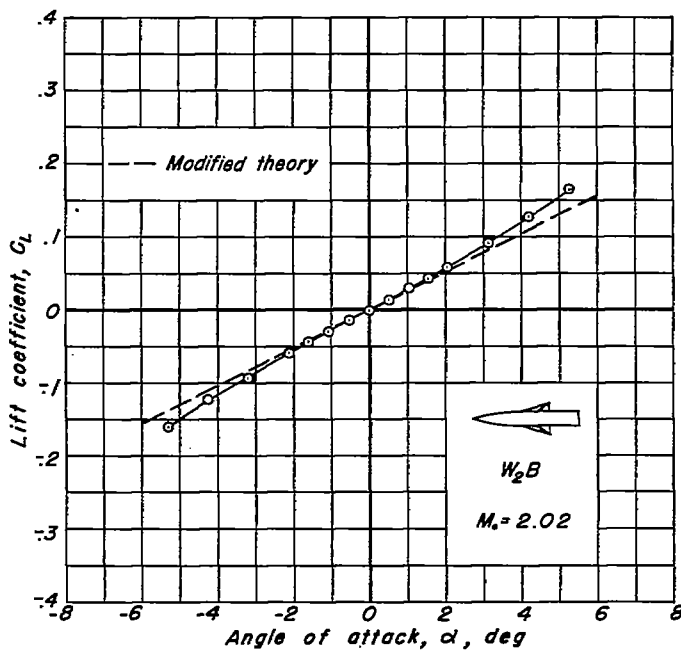
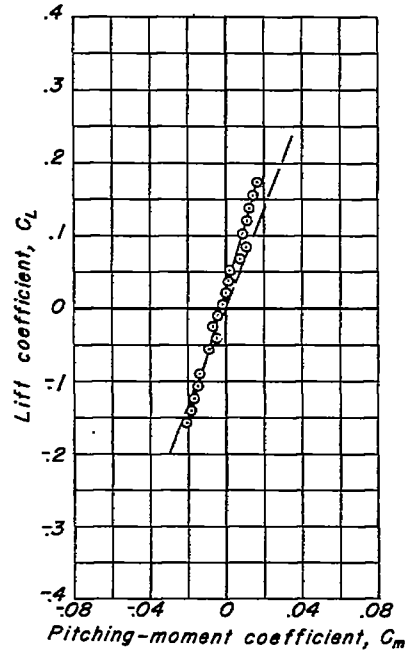
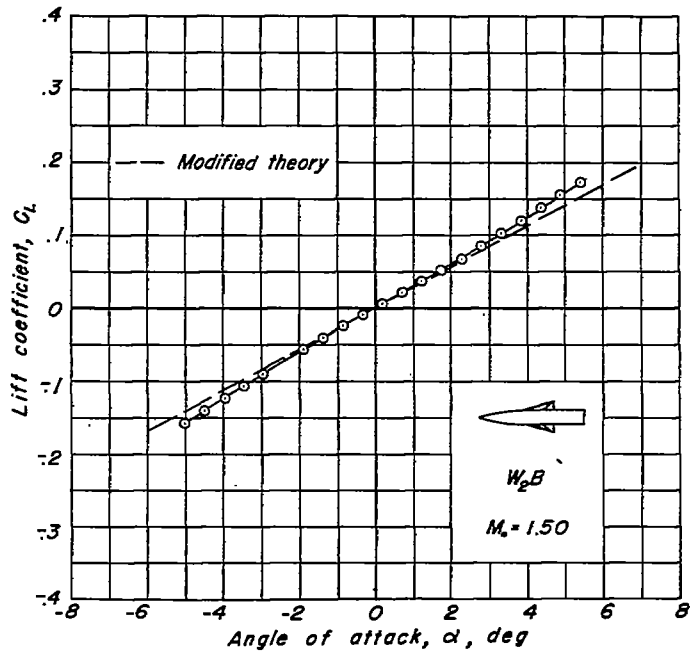


Figure 7. — Lift and moment coefficients of wing-body combinations at  $M_0 = 1.50$  and  $M_0 = 2.02$ .



(b) Combination  $W_2 B$ .

Figure 7.— Continued.

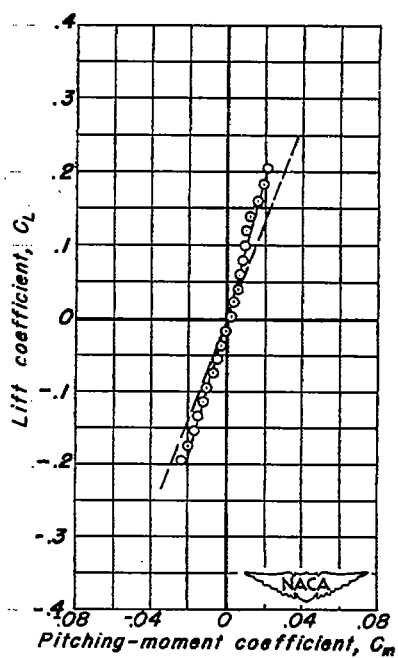
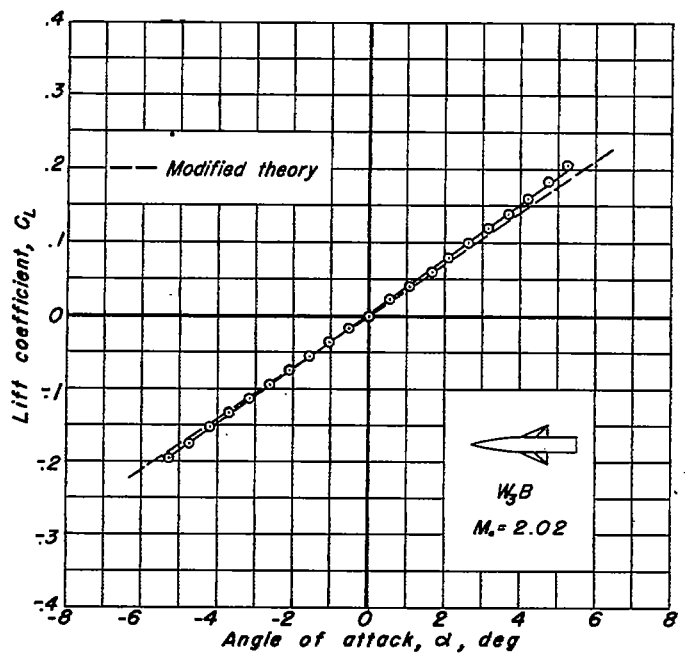
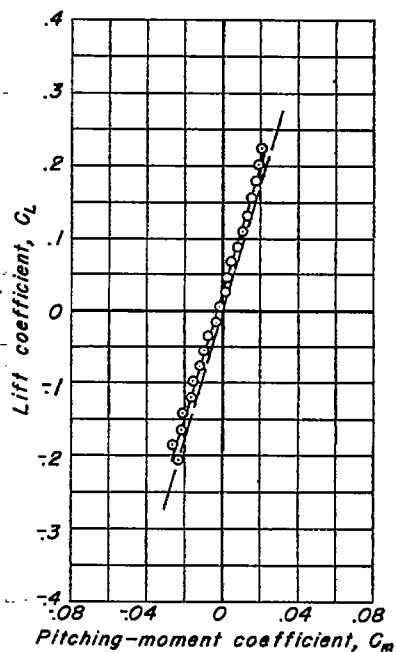
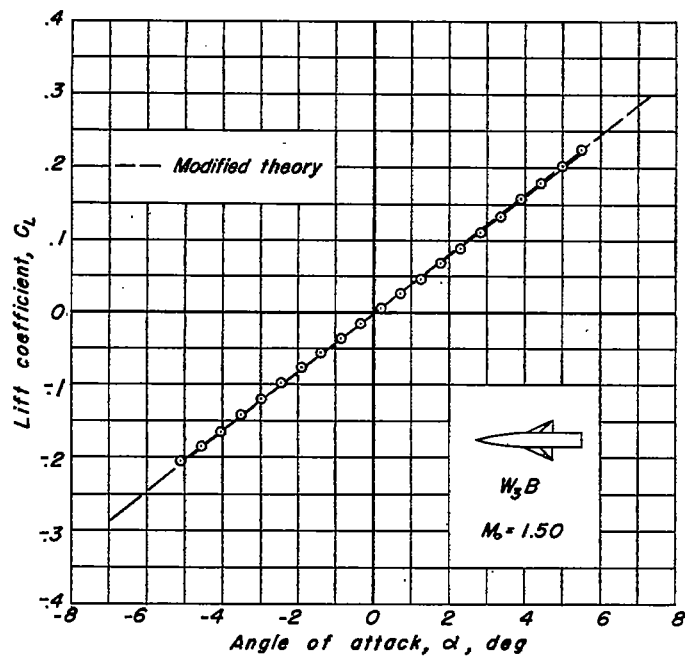
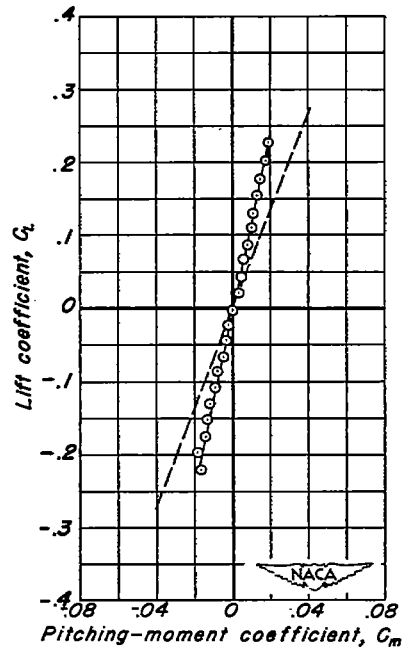
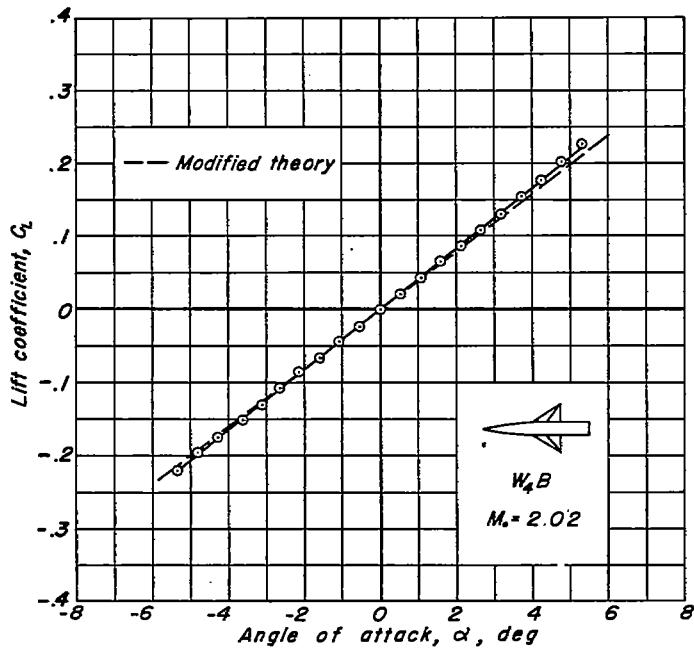
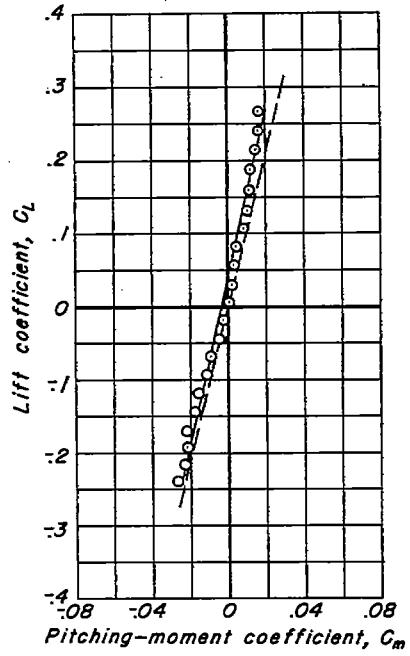
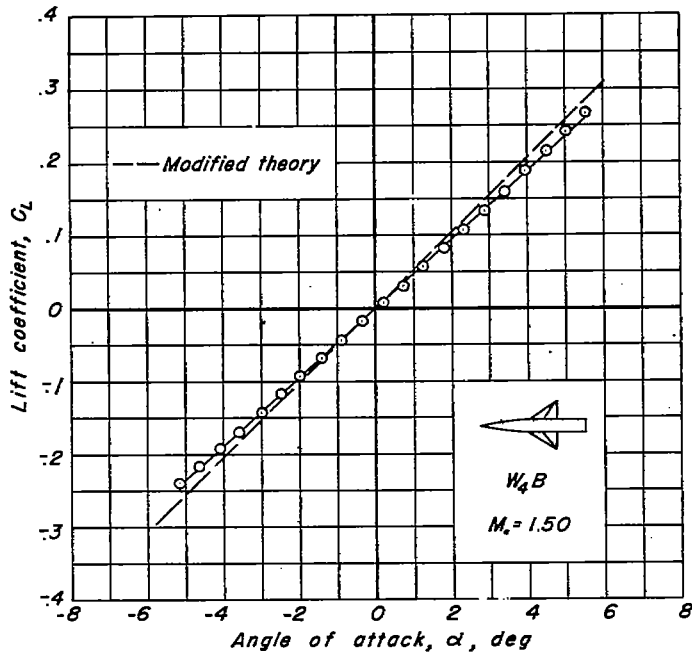


Figure 7.— Continued.

(c) Combination  $W_3B$ .



(d) Combination  $W_4 B$ .

Figure 7.— Continued.

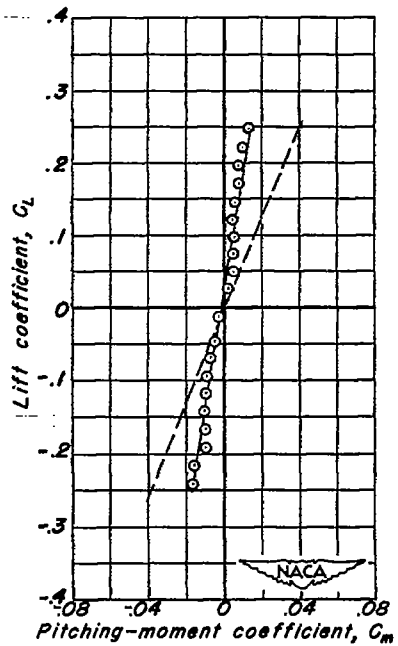
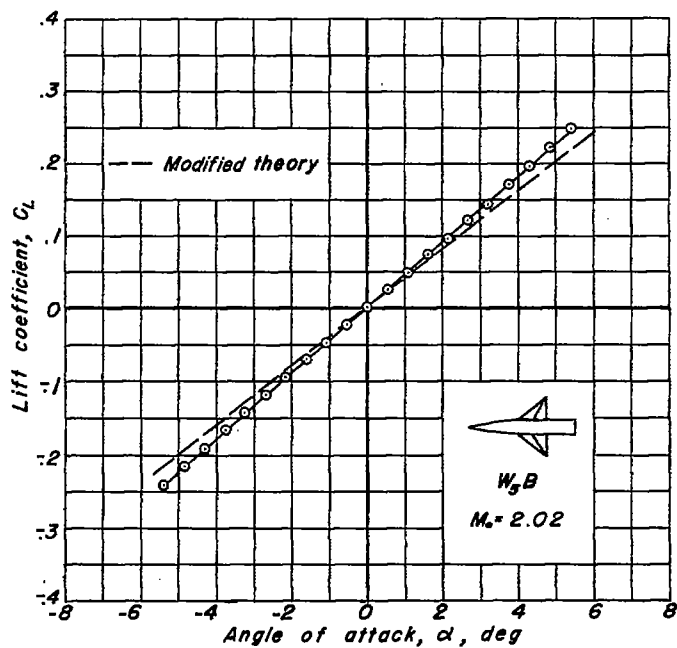
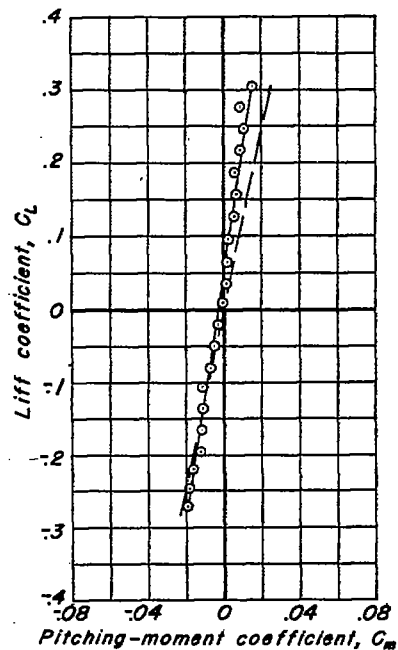
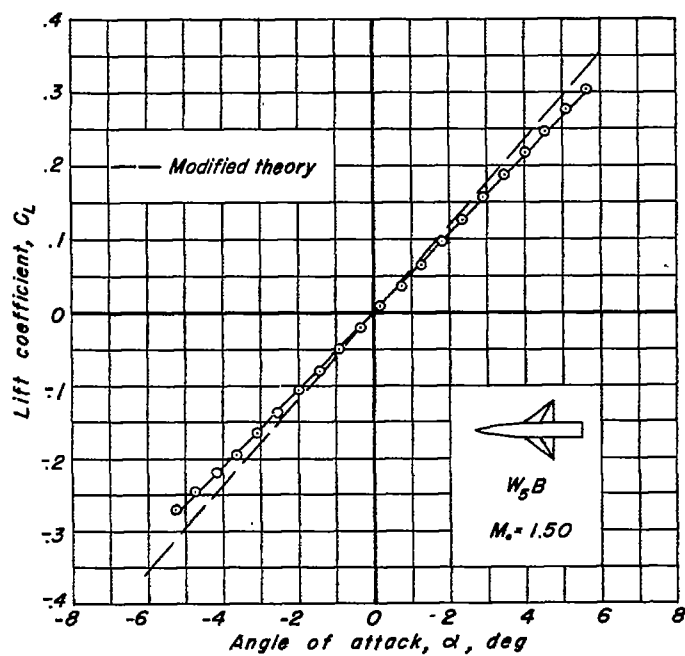
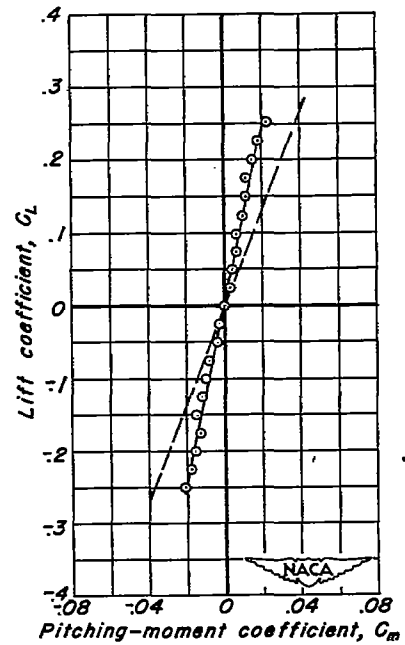
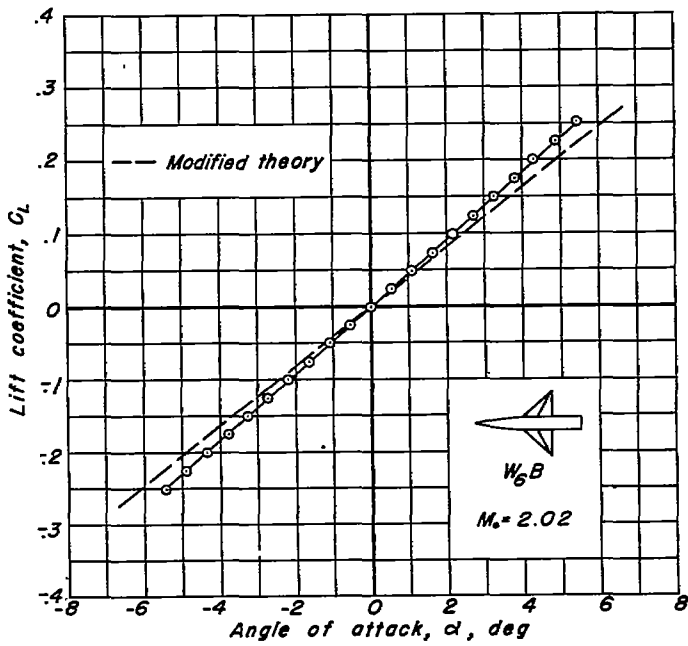
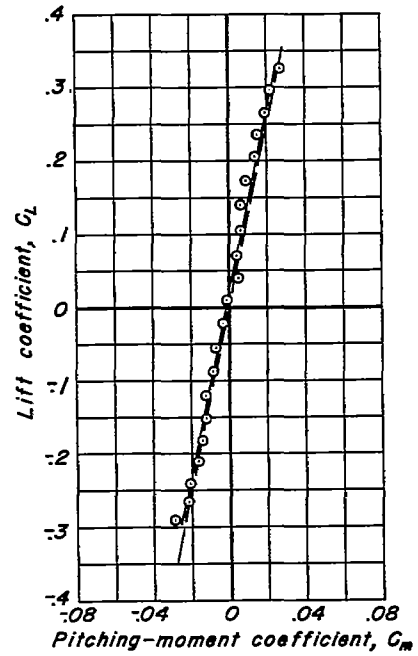
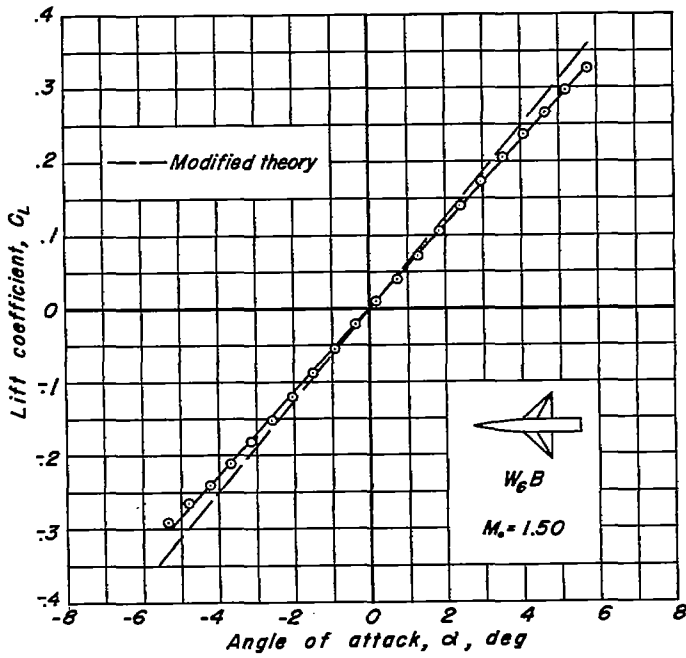
(e) Combination  $W_5 B$ .

Figure 7.— Continued.



(f) Combination  $W_6 B$ .

Figure 7.— Concluded.

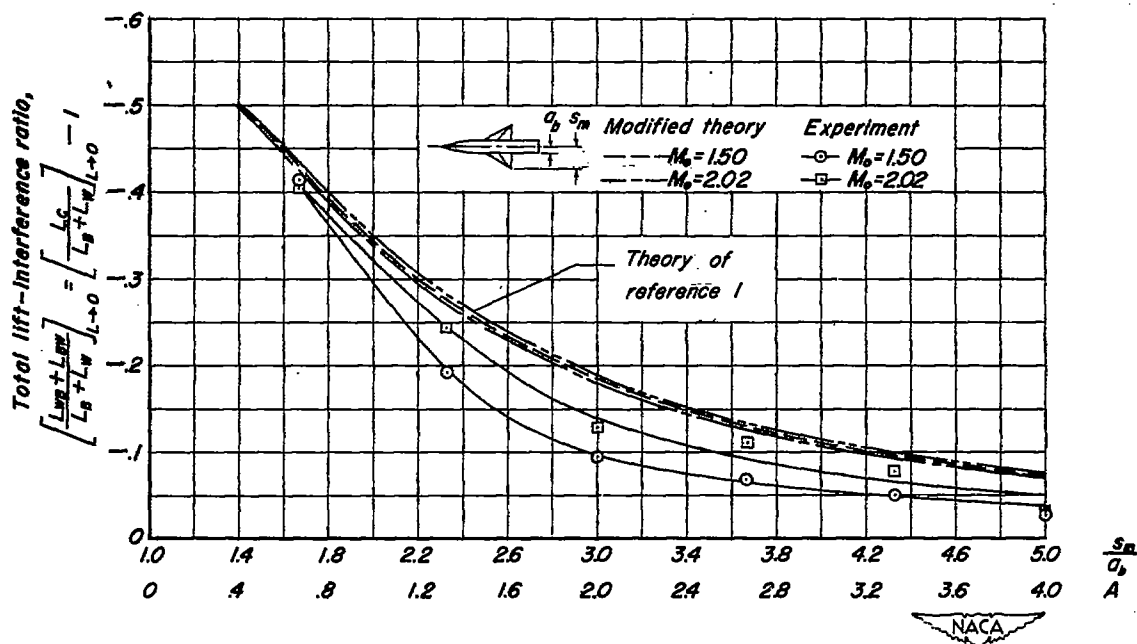


Figure 8. — Total lift-interference ratio at  $M_a=1.50$  and  $M_a=2.02$ .

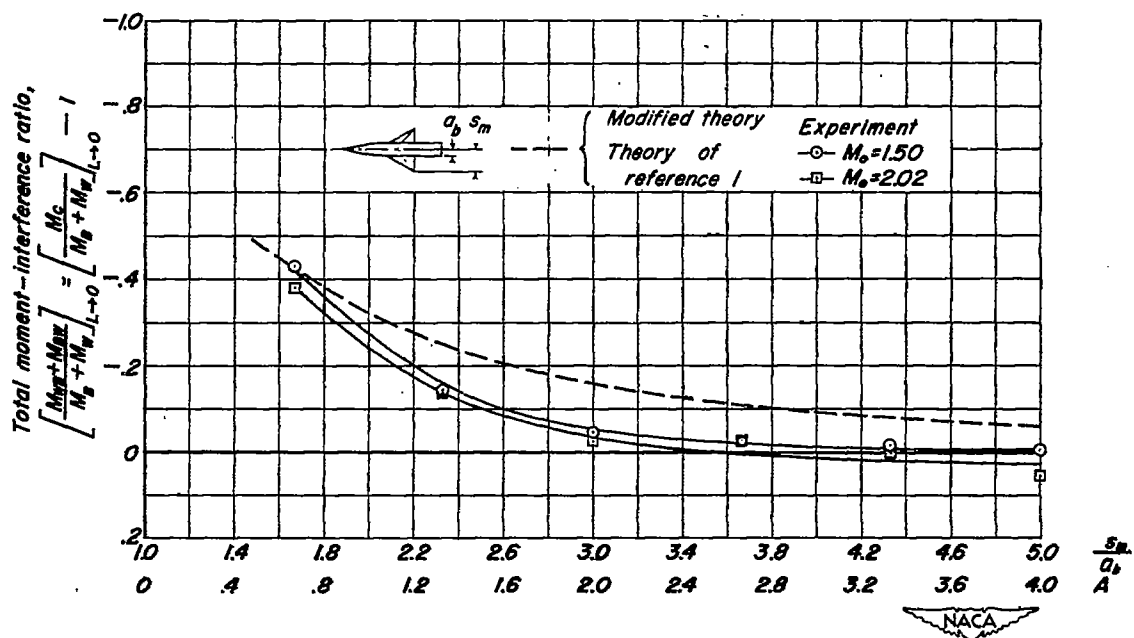


Figure 9. — Total moment-interference ratio at  $M_a=1.50$  and  $M_a=2.02$ .

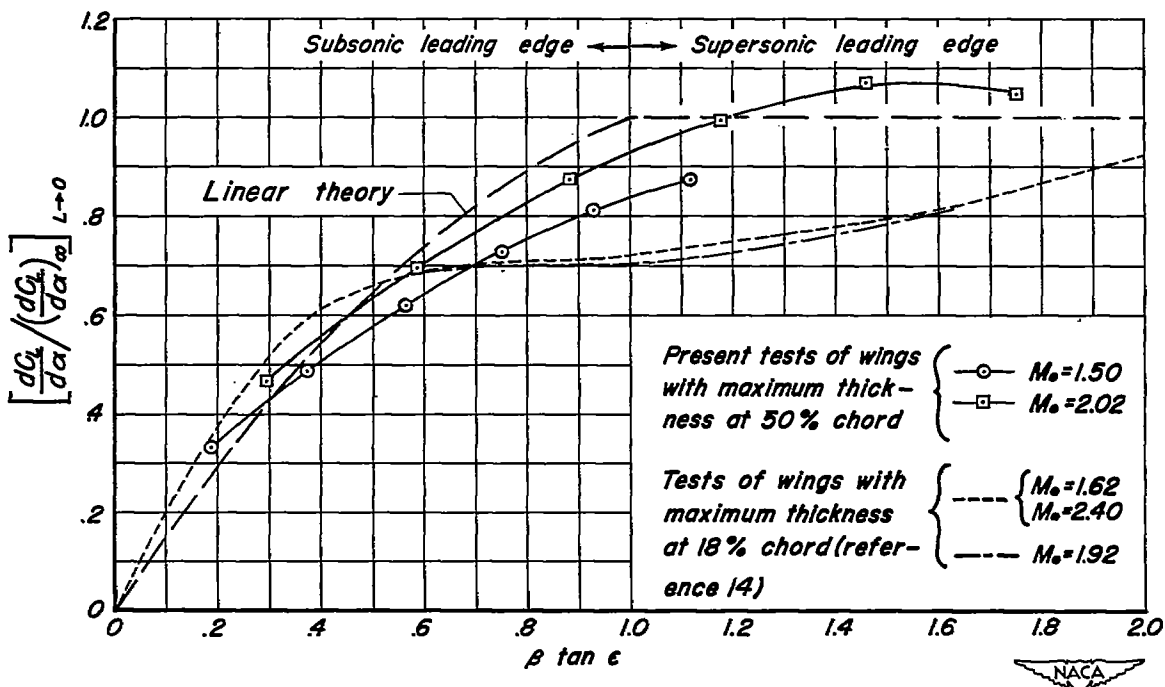


Figure 10. — Lift-curve slopes for triangular wings with maximum thickness at 50-percent chord and at 18-percent chord.

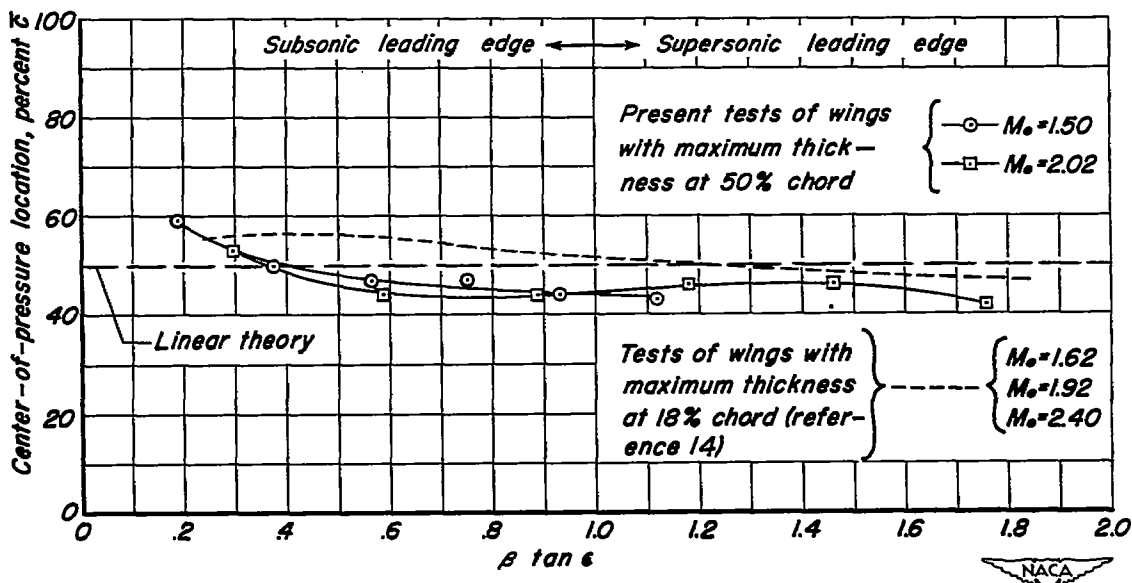


Figure 11. — Center-of-pressure locations for triangular wings with maximum thickness at 50-percent chord and at 18-percent chord.

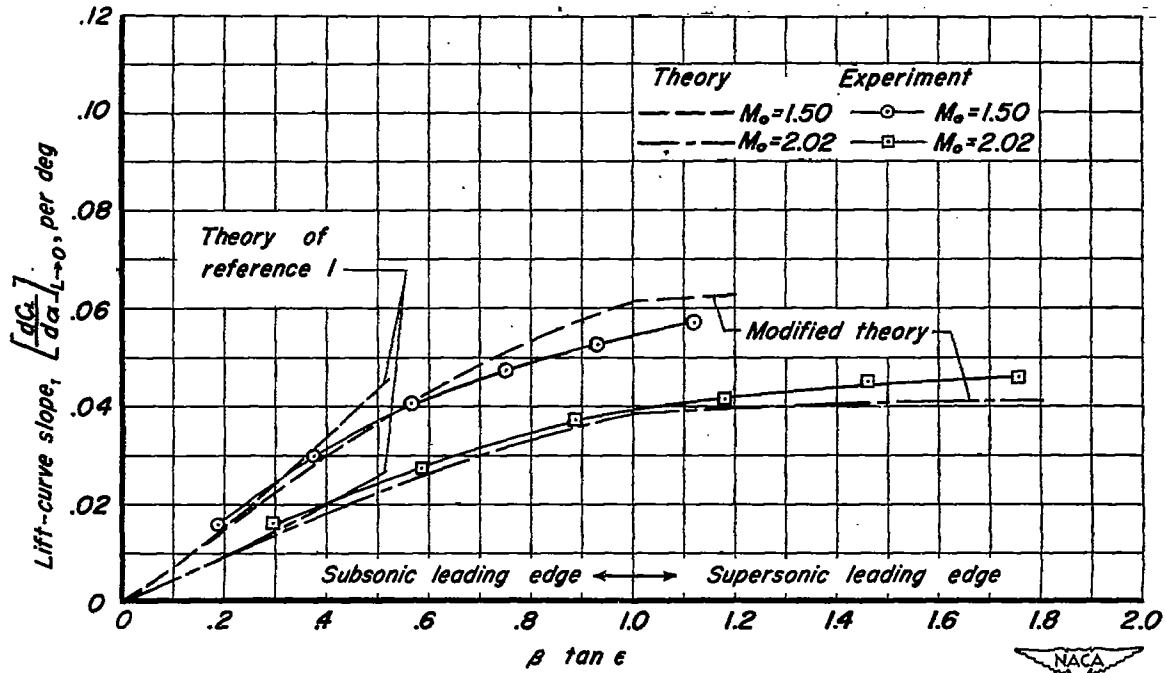


Figure 12.— Lift-curve slopes of wing-body combinations at  $M_0=1.50$  and  $M_0=2.02$ .

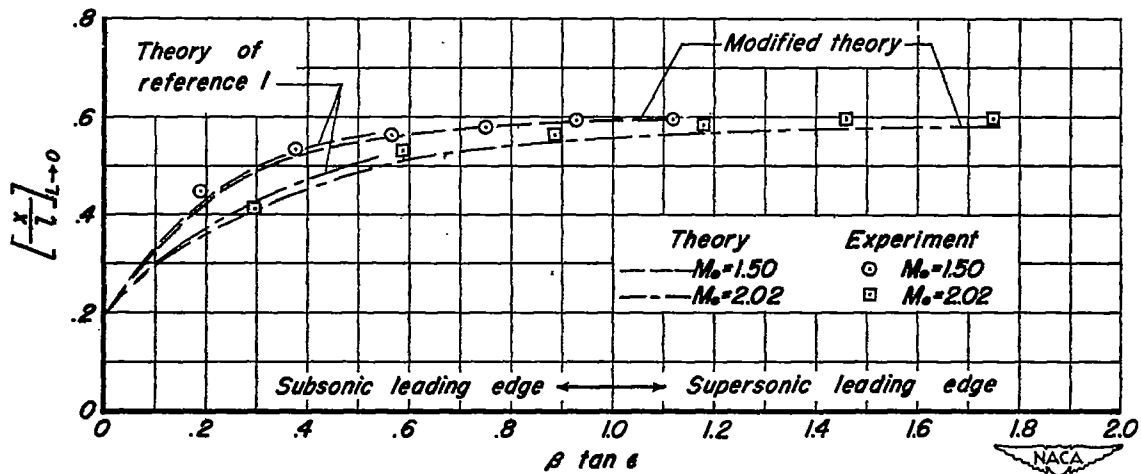


Figure 13.— Center-of-pressure positions of wing-body combinations at  $M_0=1.50$  and  $M_0=2.02$ .

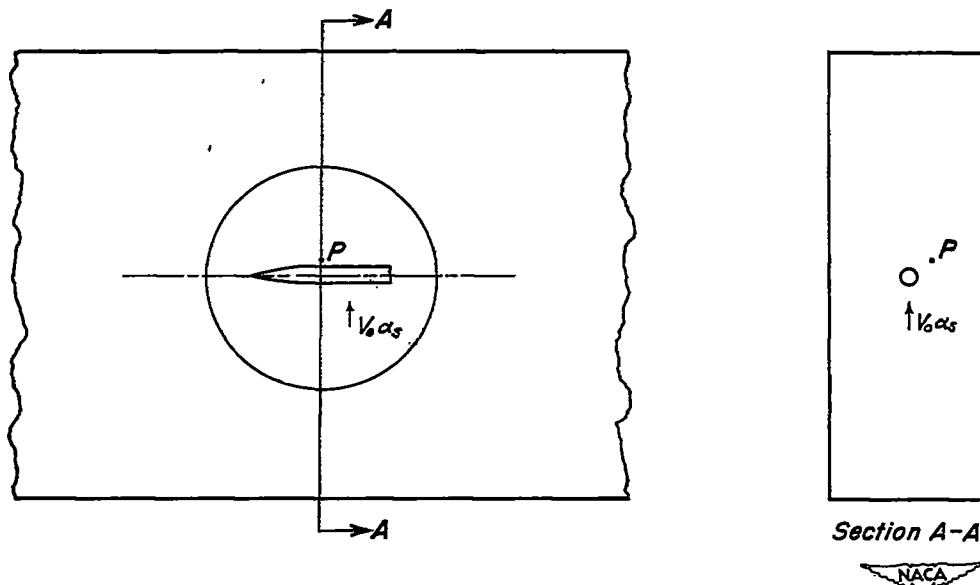


Figure 14.—View of body in tunnel, and cross-sectional view normal to body axis.

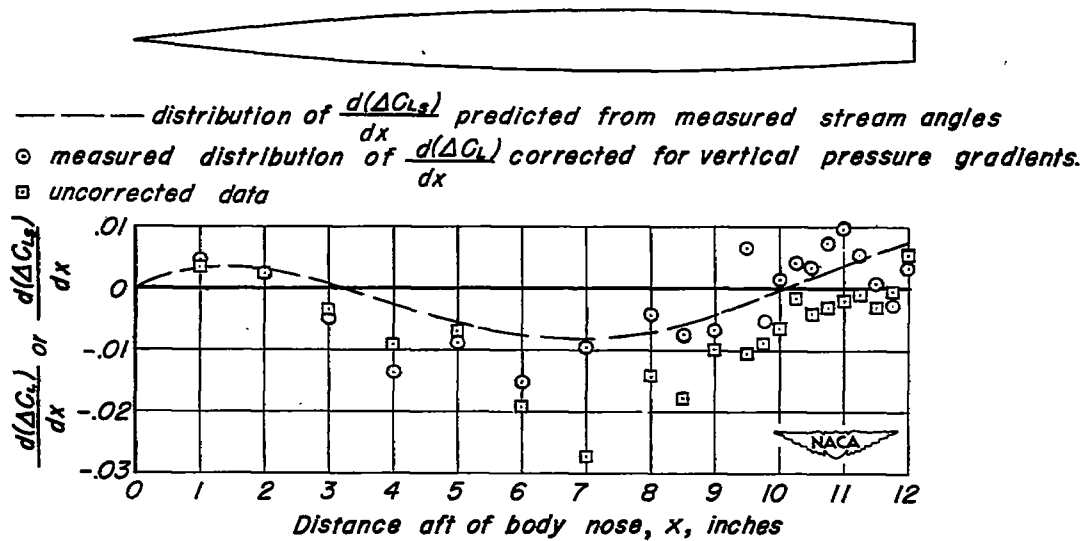


Figure 15.— Comparison between measured lift distribution corrected for vertical pressure gradients and lift distribution predicted from measured stream angles on a parabolic-arc body at zero angle of attack.